MOLECULAR AND CELLULAR BIOLOGY, July 2007, p. 4953–4967 Vol. 27, No. 13
0270-7306/07/$08.00+0 doi:10.1128/MCB.02034-06

Enhanced Polyamine Catabolism Alters Homeostatic Control of White Adipose Tissue Mass, Energy Expenditure, and Glucose Metabolism▽

Eija Pirinen,[1,2] Teemu Kuulasmaa,[1] Marko Pietilä,[2]† Sami Heikkinen,[1,2]† Maija Tusa,[1,2] Paula Itkonen,[1] Susanna Boman,[2] Joanna Skommer,[1] Antti Virkamäki,[3] Esa Hohtola,[4] Mikko Kettunen,[5] Szabolcs Fatrai,[1] Emilia Kansanen,[2] Suvi Koota,[2] Kirsi Niiranen,[2] Jyrki Parkkinen,[6] Anna-Liisa Levonen,[2] Seppo Ylä-Herttuala,[2] J. Kalervo Hiltunen,[7] Leena Alhonen,[2] Ulf Smith,[8] Juhani Jänne,[2] and Markku Laakso[1]*

Department of Medicine, University of Kuopio, FI-70211 Kuopio, Finland[1]; A. I. Virtanen Institute for Molecular Sciences, University of Kuopio, FI-70211 Kuopio, Finland[2]; Minerva Foundation Institute for Medical Research, University of Helsinki, FI-00290 Helsinki, Finland[3]; Department of Biology, University of Oulu, FI-90014 Oulu, Finland[4]; National Bio-NMR Facility, A. I. Virtanen Institute for Molecular Sciences, University of Kuopio, FI-70211 Kuopio, Finland[5]; Department of Pathology, University Hospital of Tampere, FI-33521 Tampere, Finland[6]; Biocenter Oulu and Department of Biochemistry, University of Oulu, FI-90014 Oulu, Finland[7]; and The Lundberg Laboratory for Diabetes Research, Department of Internal Medicine, Sahlgrenska University Hospital, SE-41345 Göteborg, Sweden[8]

Received 31 October 2006/Returned for modification 9 February 2007/Accepted 25 April 2007

Peroxisome proliferator-activated receptor γ coactivator 1α (PGC-1α) is an attractive candidate gene for type 2 diabetes, as genes of the oxidative phosphorylation (OXPHOS) pathway are coordinatively downregulated by reduced expression of PGC-1α in skeletal muscle and adipose tissue of patients with type 2 diabetes. Here we demonstrate that transgenic mice with activated polyamine catabolism due to overexpression of spermidine/spermine N^1-acetyltransferase (SSAT) had reduced white adipose tissue (WAT) mass, high basal metabolic rate, improved glucose tolerance, high insulin sensitivity, and enhanced expression of the OXPHOS genes, coordinated by increased levels of PGC-1α and 5′-AMP-activated protein kinase (AMPK) in WAT. As accelerated polyamine flux caused by SSAT overexpression depleted the ATP pool in adipocytes of SSAT mice and N^1,N^{11}-diethylnorspermine-treated wild-type fetal fibroblasts, we propose that low ATP levels lead to the induction of AMPK, which in turn activates PGC-1α in WAT of SSAT mice. Our hypothesis is supported by the finding that the phenotype of SSAT mice was reversed when the accelerated polyamine flux was reduced by the inhibition of polyamine biosynthesis in WAT. The involvement of polyamine catabolism in the regulation of energy and glucose metabolism may offer a novel target for drug development for obesity and type 2 diabetes.

Type 2 diabetes is a growing epidemic worldwide. Defects in insulin secretion and insulin action are fundamental disorders of this disease (30). Several mechanisms regulating insulin secretion and insulin action have been identified, but none of them is likely to explain completely the risk of type 2 diabetes. Previous studies have revealed novel mechanisms, distinct from the insulin signaling pathway, for type 2 diabetes. Mootha et al. (36) identified a set of genes involved in oxidative phosphorylation (OXPHOS), the expression of which was coordinately decreased in human diabetic muscle. Similarly, Patti et al. (40) found the downregulation of OXPHOS not only in individuals with type 2 diabetes but also in their first-degree relatives. In both of these studies, decreased peroxisome proliferator-activated receptor (PPAR) γ coactivator 1α (PGC-1α) expression was responsible for the downregulation of OX PHOS genes. In addition, the expression of PGC-1α has been shown to be downregulated in white adipose tissue (WAT) of insulin-resistant (15) and morbidly obese (50) subjects.

PGC-1α was first identified as a coactivator of PPARγ (45), and it plays a critical role in the regulation of adaptive thermogenesis. Subsequent studies have demonstrated that PGC-1α regulates mitochondrial biogenesis (49), uncoupling (45, 56), fatty acid oxidation (61), OXPHOS (36), glucose transport in muscle (35), hepatic gluconeogenesis (64), and skeletal muscle fiber-type switching (44). PGC-1α is highly expressed in brown adipose tissue (BAT), heart, and skeletal muscle and moderately expressed in liver, but a low expression level is found in WAT. The expression of PGC-1α is induced by exercise through 5′-AMP-activated protein kinase (AMPK) and calcium (2), cytokines, and leptin (65). AMPK is a heterotrimeric enzyme consisting of an α catalytic subunit and regulatory β and γ subunits (63). It is a major sensor of cellular energy state and is activated by any stress that depletes the ATP/AMP ratio, e.g., oxidative stress, hypoxia, or nutrient deprivation. Other inducers of AMPK are calcium, cytokines, leptin, adiponectin, and catecholamines (5, 16, 25). Regulation of AMPK activity involves allosteric activation by AMP and covalent modification of threonine 172 in the α subunit by phosphorylation catalyzed by upstream kinase LKB1 (23). The γ subunits play a role in determining sensitivity to AMP (8), and of the α subunits, the α2 isoform is more sensitive to AMP (48). Once activated, AMPK stimulates pathways generating ATP (glucose and fatty acid oxidation) and inhibits pathways consuming ATP (triglyceride [TG] and cholesterol biosynthesis) (63).

* Corresponding author. Mailing address: Department of Medicine, University of Kuopio, P.O. Box 1777, FI-70211 Kuopio, Finland. Phone: 358-17-172151. Fax: 358-17-173993. E-mail: Markku.Laakso@kuh.fi.
† These authors contributed equally.
▽ Published ahead of print on 7 May 2007.

The naturally occurring polyamines putrescine, spermidine, and spermine are implicated in the control of cellular growth and differentiation (21). Spermidine and spermine have been shown to mimic insulin action in glucose metabolism in isolated rat adipocytes (33). In contrast, the role of putrescine in glucose metabolism and insulin action has remained controversial (33, 51). However, the putrescine/spermine pathway has been shown to regulate mitochondrial respiratory chain activity in tumor-bearing mice (60).

In this study, we investigated transgenic (Tg) mice overexpressing spermidine/spermine N^1-acetyltransferase (SSAT) (41). SSAT is the key enzyme in the catabolism of polyamines as it is critically involved in the conversion of spermidine and spermine back to putrescine (22). The activation of polyamine catabolism leads to an accelerated flux of polyamines, an accumulation of putrescine, and a compensatory increase in the biosynthesis of polyamines by ornithine decarboxylase (ODC) due to the reduction of spermidine and/or spermine pools (22, 24). We show that SSAT mice have a reduced amount of WAT, a low tissue accumulation of TGs, a high basal metabolic rate, improved glucose tolerance, high insulin sensitivity, and overexpression of the OXPHOS pathway coordinated by high expression of PGC-1α and AMPK in WAT. The latter changes are not attributable to the hairless phenotype of SSAT mice, as revealed by parallel studies on another hairless mouse strain with an unrelated mutation. Our results support the notion that metabolic changes in SSAT mice are related to accelerated polyamine flux in adipocytes attributable to enhanced polyamine catabolism and consumption of centrally important metabolites, such as ATP.

MATERIALS AND METHODS

Animals. The generation of Tg Uku165b (DBA/2 × BALB/c) mice overexpressing SSAT under an endogenous SSAT promoter has been described previously (41). Hairless (MF1 hr/hr) or normally haired (MF1 hr/+) HsdOla mice were purchased from Harlan, United Kingdom. The animals were housed on 12-h light/dark cycle at 22 ± 1°C unless otherwise stated and were fed a regular laboratory chow. The study protocols were approved by the Animal Care and Use Committee of the University of Kuopio and the provincial government.

Histology and cell sizing of adipocytes. Tissues were removed from 2.5- to 4-month-old female and male mice and fixed in 10% formaldehyde. Fixed samples were dehydrated and embedded in paraffin. Tissues were cut into 10-μm sections, mounted on slides, and stained with hematoxylin and eosin. Adipocytes were isolated by collagenase digestion and mean cell size was determined as described previously (52). Cell density and total cell number of perigonadal fat pads were calculated according to methods previously described (28).

Analysis of body composition. Organ weights were determined for 4-week-old or 4- to 6-month-old female and male mice. Lean body mass and fat mass of 6-month-old mice were determined using high-resolution magnetic resonance imaging. For magnetic resonance imaging, the animals were sacrificed using 5% halothane in N_2O-O_2 and externally fixed to a custom-built animal holder. A chemical-shift-selective three-dimensional gradient echo pulse sequence (time to repetition, 100 ms; time to echo, 12 ms; field of view, 4 by 2.56 by 10 cm^3 covered with 400 by 128 by 128 points) was used to acquire whole-body-fat images at 4.7 T with a quadrature-type volume coil (length, 10 cm; diameter, 6 cm). Total fat was estimated from images as previously described (17).

Tissue TG concentrations. TG concentrations in skeletal muscle, liver, and heart were determined for 4-month-old, fed female SSAT and wild-type (Wt) mice after KOH hydrolysis and saponification using a microfluorometric glycerol assay method (26, 62).

Polyamine metabolites and SSAT activity. Polyamines from 3-month-old female SSAT and Wt mice were determined by using high-performance liquid chromatography (20). SSAT activity was assayed as described previously (3). SSAT activity and polyamine concentrations were normalized for DNA amount assayed by modified Burton's method (14).

Laboratory determinations. Laboratory parameters for young (4-week-old) male or adult (4-month-old) female SSAT, MF1, or Wt mice were determined before and/or after 12 to 18 h of fasting. Plasma or serum samples were taken from the saphenous or tail vein. Blood levels of serum-free fatty acids (FFAs) were measured using a TG detection kit (WAKO, Osaka, Japan), and plasma TG levels were measured colorimetrically using a Microlab 200 analyzer (Merck, Darmstadt, Germany). Plasma glucose was determined microfluorometrically (39), and plasma insulin was measured using a rat insulin enzyme-linked immunosorbent assay kit (Crystal Chem, Inc., Chicago, IL), with mouse insulin as a standard. Serum β-hydroxybutyrate was determined enzymatically using a Hitachi 717 analyzer. Glycerol levels were determined using a microfluorometric glycerol assay (62). Plasma leptin levels were analyzed using a mouse enzyme-linked immunosorbent assay kit for leptin (Crystal Chem, Inc., Chicago, IL).

Indirect calorimetry. The basal metabolic rate was measured by indirect calorimetry using a four-chamber open-flow respirometer. Animals were individually housed in specially built chambers which were constructed of acrylic (Plexiglas) tubes and resided in a darkened climatic cabinet, with an airflow of 300 ml/min (standard temperature, pressure, and dry gas) regulated by mass-flow controllers). A sample (75 ml/min) of dried outlet air was pumped into O_2 and CO_2 analyzers (Servomex 1440; Servomex, United Kingdom), and each animal was measured for 5 min during each 20-min measurement cycle. The measurements were performed using 4-month-old female and male SSAT and Wt mice after 12 h of fasting, except the determination of basal metabolic rate before and after hair loss, for which we used 2.5-week-old and 13-week-old mice without or with 4 h of fasting. All measurements were done at thermoneutrality (32.5°C). Oxygen consumption (VO_2) and carbon dioxide production (VCO_2) (ml/min) were calculated using the equations appropriate for the measurement where only water is removed before analysis (34). The respiratory quotient (RQ) was calculated as VCO_2/VO_2 in resting and active states.

Body temperature and activity. The core body temperatures and activities of SSAT and Wt mice were monitored telemetrically using intraperitoneally implanted body temperature transmitter devices (19).

Fatty acid oxidation in adipocytes and liver. Adipocytes were isolated from perigonadal fat pads by a modification of Rodbell's method (47). One milliliter of the diluted adipocyte suspension was incubated with 0.5 μCi [^{14}C]palmitate (57 μCi/μmol; Amersham Biosciences, United Kingdom) bound to 50 mg fatty acid-free albumin (Sigma, St. Louis, MO) for 30 min in test tubes at 37°C with gentle shaking. Liberated $^{14}CO_2$ was trapped into folded filter paper containing 0.5 M Solvable (Packard Instrument Company, Inc.). At the end of the incubation period, $^{14}CO_2$ produced by the adipocytes was released by injection of 0.5 ml of 10% trichloroacetic acid into the test tubes. After 15-min incubations at 37°C, each folded filter paper containing the absorbed $^{14}CO_2$ was quickly transferred into a scintillation vial with 3 ml of scintillation fluid for β-counting. Values were normalized for DNA amount assayed by modified Burton's method (14).

After 12 h of fasting, mitochondria were isolated from liver tissues of 6-month-old male Tg and Wt mice as previously described (38). The incubations were carried out with 0.5 to 1.2 mg/ml of mitochondrial protein at 30°C. β-Oxidation of palmitoylcarnitine was monitored as the rate of ferricyanide reduction, as described previously (37).

Glucose and insulin tolerance tests. A glucose tolerance test was performed on nonanesthetized, 3- to 4-month-old female SSAT and Wt mice after 12 to 13 h of fasting. After intraperitoneal injections of 2 mg D-glucose/g of body weight, blood samples were taken from the tail vein at time points of 0, 15, 30, 60, and 120 min. In the insulin tolerance test, 12- to 13-h-fasted, nonanesthetized, 3- to 4-month-old female SSAT and Wt mice were subjected to intraperitoneal injections of 0.25 mU/g insulin (Actrapid; Novo Nordisk, Denmark) or 0.15 mU/g insulin and 0.4 mg/g D-glucose. Blood samples were drawn from the tail vein at time points of 0, 20, 40, and 80 min.

Affymetrix analysis. Total RNA from perigonadal WAT of fed, 4-month-old female mice was isolated using an RNeasy mini kit (QIAGEN, Germany). The acidic guanidinium thiocyanate method (10) was used for RNA isolation from skeletal muscle and liver. Within a genotype, equal quantities of total RNA were pooled from skeletal muscle and liver or WAT from four or three mice, respectively. A hybridization mixture containing 15 μg of biotinylated cRNA was prepared according to the protocols provided by Affymetrix. Ten micrograms of biotinylated cRNA was hybridized to a mouse Affymetrix MG-U74A-v2 chip (Affymetrix, Santa Clara, CA), representing ~6,000 sequences of mouse Unigene that have been characterized functionally and ~6,000 sequences of expressed sequence tag clusters. The chips were washed and scanned according to the Affymetrix standard protocols. Signal intensities were quantitated using Affymetrix Microarray Suite 5.0. Global scaling was used to standardize signal intensities across the individual arrays. Gene expression changes in different tissues were evaluated by comparing individual arrays (two Wt and two Tg) to

each other with Affymetrix Microarray Suite 5.0 (total of four comparisons per tissue). A change in *P* value for each probe set reported by Affymetrix Microarray Suite 5.0 was scored as follows: $0.0000 \leq P \leq 0.0025$ was equivalent to a score of +10 for upregulated genes or −10 for downregulated genes and $0.0025 < P \leq 0.030$ was equivalent to a score of +5 for upregulated genes or −5 for downregulated genes. Signal changes (*n*-fold) as $\log_2$ ratios were averaged, and scores were summed. GenMAPP (11) and MAPPFinder (12) were used to identify gene expression changes in the context of the biological pathways and gene ontology. The analysis was performed using two criteria: average change (*n*-fold) as $\log_2$ ratio ($\geq$0.4 for upregulated genes and ≤ -0.4 for downregulated genes) and score ($\geq$20 for upregulated genes and ≤ -20 for downregulated genes). Z scores, which provide values for ranking the gene ontology terms, were calculated as described previously (12). A positive Z score indicates that there are more genes meeting the criterion in a gene ontology term than would be expected by random chance.

Electron microscopy. Tissue pieces from 7-month-old female SSAT and Wt mice were fixed with 2.5% glutaraldehyde and 0.1 M sodium cacodylate, pH 7.4, overnight. Postfixation was done by incubating 1% OsO_4 in 0.1 M sodium cacodylate, pH 7.4, for 2 h. After ethanol dehydration, the samples were embedded in LX-112 resin (Ladd Research Industries, Burlington, VT). Ultrathin sections (μm) were obtained with a Reichert-Jung Ultracut E ultramicrotome (Reichert-Jung, Buffalo, NY) and were contrasted with uranyl acetate and lead citrate before examination with a JEOL JEM 1200EX transmission electron microscope (JEOL, Ltd., Tokyo, Japan).

mtDNA analysis. Mitochondrial DNA (mtDNA) was quantitated by measuring the ratio of a mitochondrial gene (16S RNA) to a nuclear gene (HKII, intron 9) by quantitative real-time PCR (RT-PCR). DNA was isolated from WAT of 6-month-old female SSAT and Wt mice by use of proteinase K and phenol-chloroform–isoamyl alcohol extraction. Quantitative RT-PCRs were performed using 0.5 ng of DNA as the template, gene-specific primers and probe, and TaqMan reagents from Applied Biosystems with an ABI PRISM 7700 instrument (Applied Biosystems, Foster City, CA). Running conditions were 2 min at 50°C, 10 min at 95°C, and 40 cycles of 15 s at 95°C and 1 min at 60°C. Primers and probes were designed using an assay-by-design system (Applied Biosystems, Foster City, CA). Primer sets are available from the authors upon request.

Quantitative RT-PCR. To verify our Affymetrix results, total RNA from perigonadal WAT of 4-week-old or 4-month-old female mice was isolated using an RNeasy lipid tissue minikit (QIAGEN, Germany). Total RNA was treated with DNase I (Promega, Madison, WI) and purified using an RNeasy mini kit (QIAGEN, Germany). The absence of genomic DNA in the RNA samples was verified by a lack of PCR amplification with primers recognizing numerous GAPDH (glyceraldehyde-3-phosphate dehydrogenase) pseudogenes. Total RNA was transcribed to cDNA by use of a high-capacity cDNA archive kit (Applied Biosystems, Foster City, CA). Quantitative RT-PCRs were performed using 12 ng (RNA equivalents) of cDNA as a template, gene-specific primers and probe, and TaqMan reagents from Applied Biosystems with ABI PRISM 7700 and 7000 instruments (Applied Biosystems, Foster City, CA). Running conditions were 2 min at 50°C, 10 min at 95°C, and 40 cycles of 15 s at 95°C and 1 min at 60°C. Primers and probes were designed using an assay-by-design system (Applied Biosystems, Foster City, CA). Data were normalized to β-actin mRNA expression. Primer sets are available from the authors upon request.

Putrescine injections. Six-month-old, fed female Wt mice (CD2F1) received intraperitoneally 500 mg putrescine dihydrochloride/kg of body weight (Sigma, St. Louis, MO) twice, with a 1-h interval. Two hours before first injection of putrescine, one half of the animals were intraperitoneally pretreated with 25 mg/kg aminoguanidine dihydrochloride (AG) (Sigma, St. Louis, MO). Wt mice with or without AG (Sigma, St. Louis, MO) injections were used as controls. The animals were sacrificed 2 h after the first putrescine dihydrochloride injection, and tissue samples were collected for polyamine and quantitative RT-PCR analyses.

Differentiation of 3T3-L1 cells into adipocytes. 3T3-L1 cells (CL-173) were purchased from the American Type Culture Collection (ATCC, Manassas, VA). The cells were cultured in BioWhittaker Dulbecco's modified Eagle's medium (DMEM) (Camprex Bio Science, Walkersville, MD) containing 4.5 g/liter glucose, 10% fetal bovine serum (FBS) (HyClone Laboratories, Inc., Logan, UT), and 50 U/50 μg/ml BioWhittaker PEN-STREP solution (Cambrex Bio Science, Walkersville, MD). 3T3-L1 cells were differentiated into adipocytes according to the method of Student et al. (57).

Glucose uptake measurement. Prior to the determination of 2-deoxyglucose uptake, 3T3-L1 adipocytes were treated for 16 h with (i) 1 mM putrescine dihydrochloride (Sigma, St. Louis, MO) supplemented with or without 1 mM AG (Sigma, St. Louis, MO), (ii) 1 mM AG, or (iii) vehicle in culture medium containing 0.1% FBS (HyClone Laboratories, Inc., Logan, UT) and 50 μg/ml PEN-STREP in DMEM (Camprex Bio Science, Walkersville, MD). The cells were stimulated with insulin for 15 min at 37°C and then exposed to a mixture of 2-deoxy-[1-^{3}H]-glucose (Amersham Biosciences, Ltd., United Kingdom) and 2-deoxyglucose (Sigma, St. Louis, MO) at final concentrations of 1 μCi/ml and 200 μM, respectively. Cells were lysed with 0.2 M NaOH, and the ^{3}H activity was measured using a liquid scintillation counter (MicroBeta PLUS; Wallac, Turku, Finland). The protein concentration was determined using a BCA protein assay reagent kit (Pierce, Rockford, IL).

Immunohistochemical staining of macrophages. Nine-month-old female SSAT and Wt mice were sacrificed and perfused with phosphate-buffered saline and 4% paraformaldehyde. Perigonadal and inguinal fat pads were collected and further fixed in 4% paraformaldehyde, embedded in paraffin, and processed for histology. Immunohistochemical staining for macrophages on serial 6-μm sections was performed, as described previously (32), by use of an anti-mouse macrophage antibody (mMQ AIA31240, 1:6,500; Accurate Chemical & Scientific Corp., NY) followed by a biotinylated secondary antibody (1:200 dilution) and an avidin-biotin complex (Vectastain ABC-AP kit; Vector Laboratories, CA). For each animal, five high-power fields at ×200 magnification from each of three different sections of both perigonadal and inguinal fat pads were analyzed using image analysis software (AnalySIS; Soft Imaging System Gmbh, Münster, Germany). The number of macrophages was represented as the mean density of positive cells per measured adipose area (expressed as mm^2).

GO treatment. 3T3-L1 adipocytes were treated with 0, 5, or 10 mU/ml of glucose oxidase (GO) (Sigma, St. Louis, MO) for 16 h in culture medium containing 0.1% FBS (HyClone Laboratories, Inc., Logan, UT) and 50 μg/ml PEN-STREP in DMEM (Camprex Bio Science, Walkersville, MD). Total RNA was extracted by TRIzol (Invitrogen, Ltd., United Kingdom) and reverse transcribed into cDNA by use of M-MuLV reverse transcriptase (MBI Fermentas, Vilnius, Lithuania). Quantitative RT-PCR analyses were performed as described above.

Western blot analysis. Perigonadal WAT was homogenized in buffer containing 50 mM Tris-HCl, pH 7.6, 0.15 M NaCl, 1% Triton X-100, 1 mM phenylmethylsulfonyl fluoride in dimethyl sulfoxide, 10 mM Na_3VO_4, 100 mM NaF, 10 mM $Na_4P_2O_7$, and protease inhibitor cocktail (Roche Applied Science, Switzerland) or 25 mM Tris, pH 7.4, 0.1 mM EDTA, Halt phosphatase inhibitor cocktail (Pierce, Rockford, IL), and protease inhibitor cocktail (Roche Applied Science, Switzerland). Ten to 50 μg of protein from WAT or 8 μg of protein from BAT (used as a positive control) was boiled for 5 min, subjected to sodium dodecyl (lauryl) sulfate-polyacrylamide gel electrophoresis, and transferred onto nitrocellulose membranes. Membranes were blocked overnight with 5% nonfat dry milk in phosphate-buffered saline containing 0.1% Tween or 1% bovine serum albumin. Blots were probed with a 1/1,000 dilution of an antibody detecting the carboxyl terminus of PGC-1α (Chemicon International, Inc., Temecula, CA), the phosphorylated α subunit of AMPK (Cell Signaling Technology, Inc., Danvers, MA), dually phosphorylated p38 mitogen-activated protein kinase (MAPK) (Cell Signaling Technology, Inc., Danvers, MA), or actin (Santa Cruz Biotechnology, Inc., Santa Cruz, CA). This was followed by incubation with an appropriate horseradish peroxidase-conjugated secondary antibody. Antibody-bound protein was detected using a Western lighting chemiluminescence reagent plus detection kit (Perkin Elmer, Boston, MA) or an Immobilon Western chemiluminescent horseradish peroxidase substrate (Millipore, Billerica, MA).

ATP measurement. Adipocytes were isolated from fed, 4-month-old female SSAT and Wt mice as described above. ATP content was measured using an ATPlite one-step kit (Perkin Elmer, Boston, MA), and the results were normalized for double-stranded DNA amount analyzed using a Quant-iT PicoGreen kit (Molecular Probes, Inc., OR).

DFMO treatment. SSAT and Wt mice were weight matched for either 2-difluoromethylornithine (DFMO) or normal tap water treatment after weaning (4 to 5 weeks old), when SSAT mice start to lose their hair. DFMO (a gift from Ilex Oncology, Inc., TX), 0.5%, was given in the drinking water ad libitum for 2, 4, or 5 weeks. Upon termination of the experiment, the animals were sacrificed after 4 h or 12 h of fasting and tissues were taken for ATP measurement or polyamine and quantitative RT-PCR analyses, respectively. All analyses were performed as described above except that isolated total RNA was treated with a DNA-free kit (Ambion, Inc., Austin, TX).

Nutrient deprivation in fetal fibroblasts. Isolation of primary fibroblasts from Wt fetuses was performed as previously described (1), with slight modifications. Prior to experimentation, cells were cultured in DMEM with glutamine (no. 52100-039; Gibco, United Kingdom) supplemented with 2 mM L-glutamine, 10% FBS (Gibco, United Kingdom), and 50 μg/ml gentamicin. Cells were maintained at 37°C in 95% air and 5% carbon dioxide in 100-mm plates. For the nutrient deprivation experiment, cells were transferred to six-well plates and incubated in glucose- and sodium pyruvate-free DMEM with glutamine (no. 11966; Gibco,

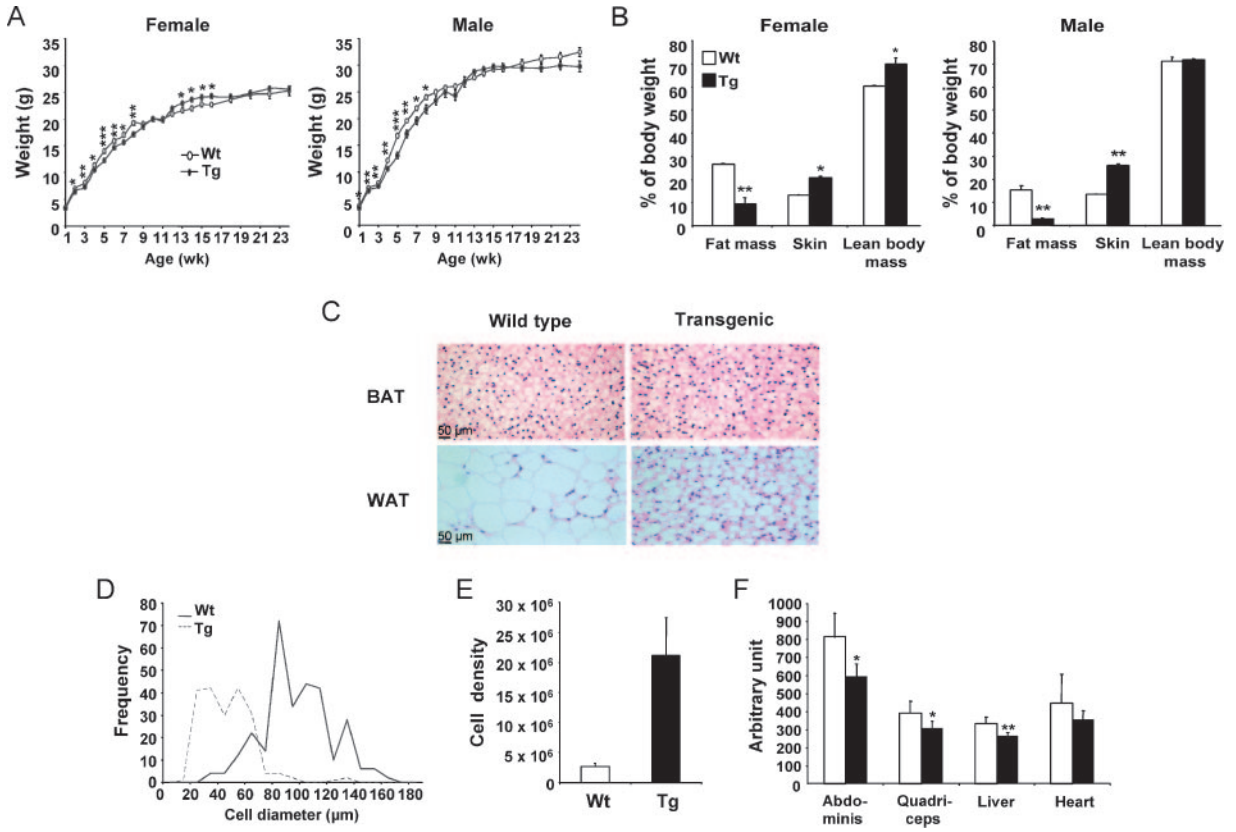

FIG. 1. Weight development and characteristics of body composition and WAT in SSAT mice. (A) Female and male SSAT and Wt mice were weighed, and the data were collected using 1- or 2-week intervals. Data are means ± SEM from 13 to 26 mice. *, $P < 0.05$; **, $P < 0.01$; ***, $P < 0.001$. (B) Body compositions of SSAT and Wt mice were determined by magnetic resonance imaging. Skin weight was obtained after dissection of skin. All values are means ± SEM from three mice per group. *, $P < 0.05$; **, $P < 0.01$. (C) Histology of intrascapular BAT and perigonadal WAT in female SSAT and Wt mice. Adipocytes were photographed at ×20 magnification. (D and E) Cell diameters and densities (cell number per g tissue) of isolated adipocytes from perigonadal fat pads of male SSAT and Wt mice. Results are presented as means from two pools of SSAT mice (six mice per pool) and from three individual Wt mice. (F) TG contents in different tissues of female SSAT (black bars) and Wt (white bars) mice. Results are expressed as means ± SEM from 10 mice per genotype. *, $P < 0.05$; **, $P < 0.01$.

United Kingdom) supplemented with 10% dialyzed FBS (Gibco, United Kingdom) and 50 μg/ml gentamicin. Cells were treated with or without 10 μM N^1,N^{11}-diethylnorspermine (DENSPM) for 24 and 48 h. Only early-passage cells were used for the experiments. ATP and SSAT measurements were performed as described above except that the results were normalized for cell number or protein amount, respectively. Cells were counted using a Coulter particle counter (Beckham, Fullerton, CA), and protein concentrations were analyzed using a Bradford protein assay reagent (Bio-Rad Laboratories, Inc., Hercules, CA).

Statistical analyses. Statistical analyses were performed using Student's *t* test (two-tailed) except that one-way or two-way analysis of variance was used for multiple comparisons. A *P* value of less than 0.05 was considered significant. Data are expressed as means ± standard errors of the means (SEM). Insulin levels were logarithmically transformed for statistical analyses.

Microarray data accession number. Affymetrix data have been published in the ArrayExpress repository (http://www.ebi.ac.uk/arrayexpress/) under the accession number E-MEXP-165.

RESULTS

Growth and body composition of SSAT mice. At the age of 1 week, female SSAT mice were indistinguishable in size from Wt mice but male SSAT mice had lower body weight than Wt mice (Fig. 1A). By the second postnatal week, SSAT mice were smaller than the corresponding Wt mice, and they remained underweight until 8 weeks (Fig. 1A). However, female SSAT mice were heavier than Wt mice from 13 to 16 weeks; otherwise, body weights were similar in adult female and male SSAT and Wt mice (Fig. 1A).

Autopsies of SSAT mice revealed markedly reduced subcutaneous and visceral fat depots. Perigonadal WAT mass was significantly reduced in 4-month-old adult and 4-week-old young (before total hair loss) SSAT mice of both genders in comparison with that of Wt mice, but there was no difference in the weights of intrascapular BAT (Table 1). Whole-body fat mass was also significantly lower in adult SSAT mice of both genders, but lean body mass was increased only in female SSAT mice (Fig. 1B). In contrast, the weight of skin was increased in adult female and male SSAT mice (Fig. 1B). Internal organs of adult female SSAT mice were significantly enlarged (Table 1), whereas adult male SSAT mice had only enlarged spleens (Table 1). In contrast, we did not observe any changes in the sizes of internal organs in young SSAT mice, except for the hearts, which were significantly enlarged in male SSAT mice (Table 1).

Histological analyses of perigonadal fat pads and isolated adipocytes showed that the cell diameter was about twofold smaller in adult SSAT mice than in Wt mice (Fig. 1C and D)

TABLE 1. Organ weights of female and male SSAT and Wt mice

Mouse group (age)	Organ wt (% of body wt)[a]						
	Peri WAT	Intra BAT	Liver	Pancreas	Spleen	Heart	Kidney
Wt female (4 mo)	3.7 ± 0.5	0.78 ± 0.07	3.8 ± 0.2	0.65 ± 0.03	0.30 ± 0.02	0.44 ± 0.01	0.46 ± 0.02
SSAT female (4 mo)	1.1 ± 0.1**	0.69 ± 0.13	4.8 ± 0.2*	0.75 ± 0.02*	0.58 ± 0.02*	0.53 ± 0.02*	0.55 ± 0.01*
Wt male (4 mo)	2.6 ± 0.3	0.69 ± 0.04	4.3 ± 0.3	ND	0.26 ± 0.01	0.53 ± 0.01	0.70 ± 0.02
SSAT male (4 mo)	0.7 ± 0.1***	0.59 ± 0.02	4.6 ± 0.1	ND	0.50 ± 0.05**	0.56 ± 0.02	0.73 ± 0.03
Wt female (4 wk)	0.36 ± 0.05	0.54 ± 0.02	4.2 ± 0.1	0.80 ± 0.02	0.72 ± 0.07	0.57 ± 0.01	0.58 ± 0.01
SSAT female (4 wk)	0.13 ± 0.01*	0.55 ± 0.04	4.0 ± 0.1	0.76 ± 0.06	0.52 ± 0.04	0.63 ± 0.04	0.61 ± 0.01
Wt male (4 wk)	0.52 ± 0.05	0.43 ± 0.03	4.6 ± 0.1	0.64 ± 0.06	0.64 ± 0.08	0.55 ± 0.01	0.67 ± 0.01
SSAT male (4 wk)	0.18 ± 0.05**	0.41 ± 0.02	4.3 ± 0.2	0.76 ± 0.02	0.46 ± 0.07	0.62 ± 0.02*	0.68 ± 0.01

[a] Data are expressed as means ± SEM from three to nine mice per gender per genotype. Peri WAT, perigonadal WAT; intra BAT, intrascapular BAT; ND, not determined. *, $P < 0.05$; **, $P < 0.01$; ***, $P < 0.001$. All other P values were NS.

and that cell density was increased by a factor of 8 (Fig. 1E). However, the total cell numbers of perigonadal fat pads were similar (Tg, $3.2 \times 10^6 \pm 0.2 \times 10^6$; Wt, $3.3 \times 10^6 \pm 0.1 \times 10^6$) due to reduced fat mass. A histological examination of intrascapular BAT (Fig. 1C) and internal organs (data not shown) did not reveal any differences between adult SSAT and Wt mice, as has been published previously (41).

Because the lack of adipose tissue causes ectopic lipid accumulation in insulin-sensitive tissues, we determined TG concentrations in skeletal muscle, livers, and hearts of adult female SSAT and Wt mice in a fed state. SSAT mice showed about 20 to 25% lower TG content in all tissues studied than Wt mice (Fig. 1F).

Polyamine pools and SSAT activity in WAT of SSAT mice. SSAT mice displayed the highest SSAT activity in WAT compared with activities in other organs (reported as pmol/μg DNA/10 min): WAT, 8.2 ± 1.7; ileum, 6.6 ± 1.1; pancreas, 6.1 ± 0.6; jejunum, 3.7 ± 0.6; lung, 2.1 ± 0.2; spleen, 1.9 ± 0.2; colon, 1.9 ± 0.1; brain, 1.6 ± 0.2; liver, 1.1 ± 0.2; kidney, 0.8 ± 0.1; skeletal muscle, 0.7 ± 0.2; heart, 0.3 ± 0.1; and BAT, 0 ± 0. Compared with that for Wt mice, SSAT activity was elevated about 220-fold in WAT of SSAT mice (Tg, 8.2 ± 1.7 pmol/μg DNA/10 min; Wt, 0.04 ± 0.04 pmol/μg DNA/10 min [$P < 0.01$]). Putrescine concentrations were elevated about 22-fold in WAT from SSAT mice in comparison with concentrations in WAT from Wt mice (Tg, 176 ± 26 pmol/μg DNA; Wt, 8 ± 2 pmol/μg DNA [$P < 0.05$]). Spermidine levels were unchanged (Tg, 101 ± 6 pmol/μg DNA; Wt, 96 ± 14 pmol/μg DNA [P was nonsignificant] [NS]), but spermine levels (Tg, 23 ± 1 pmol/μg DNA; Wt, 43 ± 5 pmol/μg DNA [$P < 0.05$]) were significantly reduced in WAT of SSAT mice.

Increased energy expenditure in SSAT mice. SSAT mice had higher oxygen consumption than Wt mice (Fig. 2A). The results remained essentially similar when expressed as $V\dot{O}_2$/lean body mass (Fig. 2A). We also measured basal energy expenditure in the same mice before (at the age of 2.5 weeks) and after (at the age of 13 weeks) hair loss. Oxygen consumption was significantly higher in SSAT mice than in Wt mice at both ages (Fig. 2B).

RQs, the ratios of carbon dioxide produced to oxygen consumed, were similar in both genotypes after fasting in the resting state irrespective of age (Tg 6-month-old mice, 0.84 ± 0.01; Wt 6-month-old mice, 0.86 ± 0.01; Tg 3-month-old mice, 0.74 ± 0.01; Wt 3-month-old mice, 0.77 ± 0.02). However, after fasting in the active state, 6-month-old SSAT mice showed significantly lower RQs (Tg, 0.82 ± 0.01; Wt, 0.86 ± 0.01 [$P < 0.05$]). In addition, SSAT mice had lower RQs in the fed and resting state (Tg, 0.75 ± 0.03; Wt, 0.82 ± 0.01 [P was NS]) but the difference was not significant.

Consistent with increased energy expenditure, 4-month-old female SSAT mice had significantly higher food and water intake (Fig. 2C) than Wt mice.

Due to increased energy expenditure, we also telemetrically studied body temperatures and physical activities of SSAT and Wt mice. At 25°C, SSAT mice had body temperatures similar to or somewhat higher than those of Wt mice during the daytime (Tg, 36.5 ± 0.1°C; Wt, 36.3 ± 0.1°C [P was NS]) and lower than those of Wt mice during the nighttime (Tg, 36.8 ± 0.1°C; Wt, 37.2 ± 0.1°C [$P < 0.05$]), but the mean temperatures over 24 h did not differ between SSAT mice and Wt mice (Tg, 36.6 ± 0.1°C; Wt, 36.8 ± 0.1°C [P was NS]). The locomotor activity of Wt mice was substantially increased during the nighttime, whereas SSAT mice did not show any significant circadian change in their activity patterns (Fig. 2D).

As oxygen consumption is determined largely by fatty acid oxidation and mitochondrial activity, we investigated β-oxidation rates in WAT, skeletal muscle, and liver. Palmitate oxidation in isolated adipocytes of female SSAT mice was markedly increased compared with that for Wt mice (Fig. 2E). In contrast, palmitate oxidation levels in tissue homogenates or isolated mitochondria of skeletal muscle did not differ between the groups (data not shown). Furthermore, palmitoylcarnitine oxidation, monitored as the rate of ferricyanide reduction, was slightly but not significantly reduced in isolated mitochondria from the livers of SSAT mice (Tg, 34.0 ± 7.21 nmol/mg protein; Wt, 39.2 ± 4.7 nmol/mg protein [P was NS]).

Biochemical measurements of SSAT mice in fed and fasting states. In a fed state, FFA and 3-hydroxybutyrate levels did not differ between adult SSAT and Wt mice, whereas leptin, glucose, and insulin levels were significantly lower and TG levels higher in adult SSAT mice than in Wt mice (Table 2). In the fasting state, all parameters measured were reduced in adult SSAT mice compared with parameters in Wt mice, with the exception of FFA levels (Table 2). In young, 4-week-old male

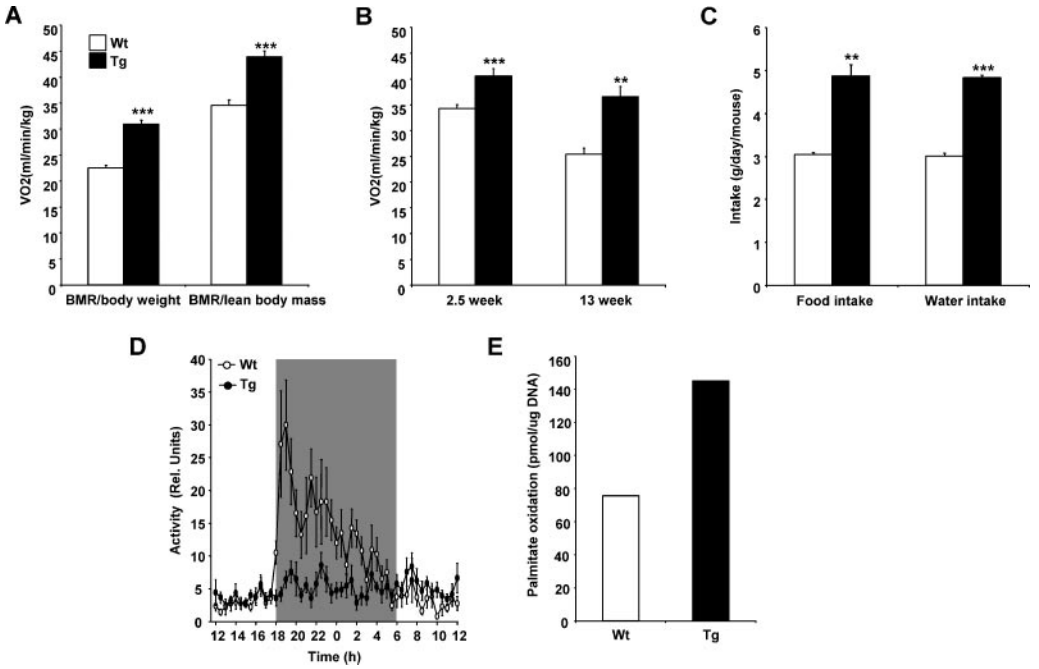

FIG. 2. Energy expenditure of SSAT and Wt mice. (A) Oxygen consumption was measured, using indirect calorimetry, for 6-month-old female and male SSAT and Wt mice after fasting. Results are expressed per body weight or lean body mass. Data are means ± SEM from 15 to 16 mice per genotype. ***, $P < 0.001$. BMR, basal metabolic rate. (B) Oxygen consumption measured before (2.5 weeks) and after (13 weeks) hair loss in female and male SSAT and Wt mice in the fasting state. Data are means ± SEM for seven to eight mice. **, $P < 0.01$; ***, $P < 0.001$. (C) Food and water intake was measured in 4- to 6-month-old female SSAT and Wt mice. Mice were housed five to eight per cage, and food and water consumption was measured after 1 week. Results are expressed as means ± SEM from 19 mice per group. **, $P < 0.01$; ***, $P < 0.001$. (D) Locomotor activities of female and male SSAT and Wt mice were monitored telemetrically at 25°C during a 12-h light/dark cycle. The gray color indicates nighttime. Results are expressed as means ± SEM from six mice per group. Rel. Units, relative units. (E) Palmitate oxidation was determined as CO_2 production in a pool of isolated adipocytes from female (5 to 13 mice per group) SSAT and Wt mice in a fed state.

mice, fed glucose levels tended to be lower than those for Wt mice (Tg, 8.9 ± 0.8 mM; Wt, 9.8 ± 0.3 mM [P was NS]). In contrast, fed insulin levels were significantly reduced (Tg, 0.33 ± 0.04 ng/ml; Wt, 0.68 ± 0.13 ng/ml [$P < 0.05$]).

Improved glucose tolerance and insulin sensitivity in SSAT mice. In the glucose tolerance test at 15, 30, 60, and 120 min after glucose administration, plasma glucose was significantly lower in SSAT mice than in Wt mice (Fig. 3A). In addition, insulin levels were lower in SSAT mice at 0 and 120 min (Fig. 3B). Insulin sensitivity, evaluated by two different intraperitoneal insulin tolerance tests (Fig. 3C and D), showed that SSAT mice were more insulin sensitive than Wt mice, as their plasma glucose levels were lower at 20, 40, and 80 min.

Enhanced expression of genes involved in the OXPHOS pathway. In order to elucidate the molecular mechanisms leading to the phenotype of SSAT mice, we analyzed gene expression profiles from WAT, skeletal muscle, and livers of fed SSAT and Wt mice by use of Affymetrix analysis. Of 12,000 sequences represented in the array, 643 in WAT, 610 in skeletal muscle, and 789 in liver were differentially expressed in SSAT mice compared with Wt mice. According to the MAPPFinder program, the number of changes was highest in WAT and the top-ranked cellular components of WAT were mitochondrion, cytoplasm, and mitochondrial matrix (Z scores of 11.2, 4.6, and 3.6, respectively). In addition, the top-ranked metabolic pathways or process terms relevant to the phenotype of SSAT mice in WAT were oxidoreductase, pyruvate metabolism, energy derivation by oxidation of organic compounds, lipid metabolism, glucose metabolism, polyamine biosynthesis, electron transport, and

TABLE 2. Blood metabolites of female SSAT and Wt mice in fed and fasting states[a]

State and mouse group	FFA (mM)	TG (mM)	β-Hydroxy-butyrate (mM)	Glycerol (mM)	Leptin (ng/ml)	Glucose (mM)	Insulin (ng/ml)
Fed							
Wt	0.43 ± 0.04	2.6 ± 0.2	0.09 ± 0.04	0.80 ± 0.04	7.2 ± 1.5	10.7 ± 0.2	1.8 ± 0.1
SSAT	0.37 ± 0.05	3.6 ± 0.2***	0.08 ± 0.03	0.81 ± 0.03	1.4 ± 0.3*	9.4 ± 0.3**	1.0 ± 0.2**
Fasting							
Wt	0.67 ± 0.05	1.4 ± 0.1	2.45 ± 0.42	1.16 ± 0.12	2.9 ± 0.8	10.3 ± 0.4	0.6 ± 0.2
SSAT	0.72 ± 0.06	1.0 ± 0.1*	0.58 ± 0.43***	0.88 ± 0.05*	0.3 ± 0.1*	8.5 ± 0.2***	0.3 ± 0.1*

[a] Results are expressed as means ± SEM for 7 to 15 mice per genotype. *, $P < 0.05$; **, $P < 0.01$; ***, $P < 0.001$. All other P values were NS.

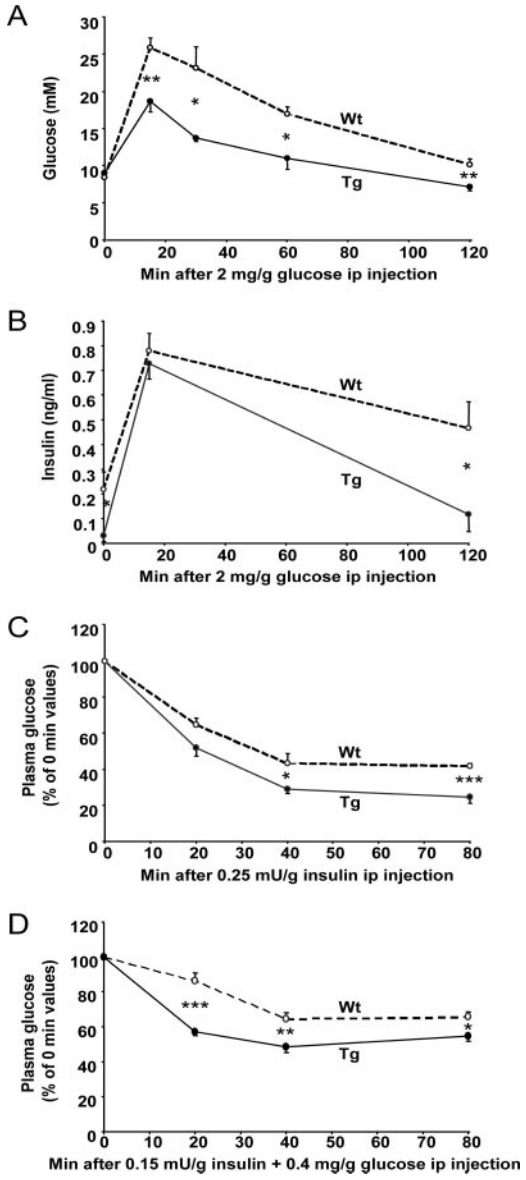

FIG. 3. Glucose tolerance and insulin sensitivity of SSAT and Wt mice. An intraperitoneal (ip) glucose tolerance test with 2 mg/mg glucose was performed on fasted, nonanesthetized, 3- to 4-month-old female SSAT and Wt mice. (A) Glucose and (B) insulin concentrations during the intraperitoneal glucose tolerance test. Intraperitoneal insulin tolerance tests with (C) 0.25 mU/g insulin and (D) 0.15 mU/g insulin and 0.4 mg/g glucose were performed on fasted, nonanesthetized, 3- to 4-month-old female SSAT and Wt mice. Results are presented as means ± SEM from five to six mice per group. *, $P < 0.05$; **, $P < 0.01$; ***, $P < 0.001$.

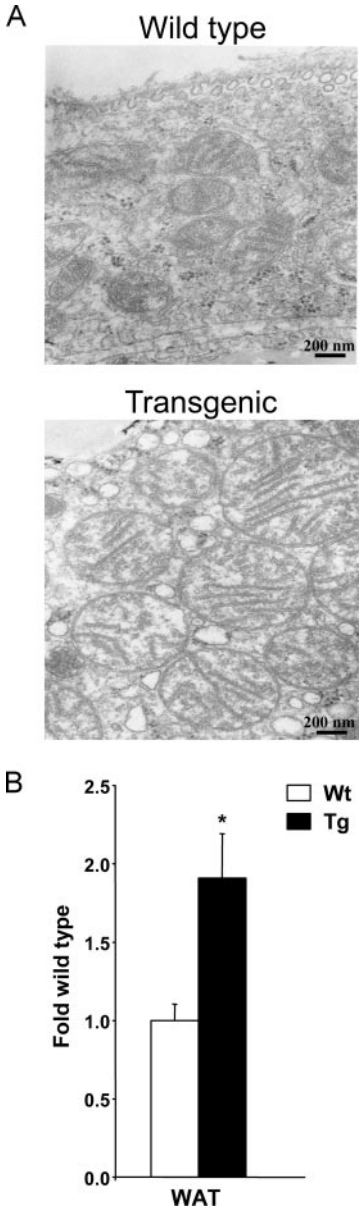

FIG. 4. Transmission electron microscopy results showing mitochondria and amounts of mtDNA in WAT of female SSAT and Wt mice. (A) Electron microscopy of mitochondria in WAT of 7-month-old female SSAT and Wt mice. Mitochondria from eight SSAT and Wt mice were photographed at ×25,000 magnification. (B) mtDNA amounts in female 6-month-old SSAT and Wt mice, analyzed by quantitative RT-PCR. Results are presented as means ± SEM from six to seven mice per group. *, $P < 0.05$.

tricarboxylic acid cycle (Z scores of 9.3, 7.3, 6.4, 5.8, 5.3, 5.0, 5.0, and 5.0, respectively).

Mitochondrial analyses. Based on the MAPPFinder results, we investigated mitochondria in WAT of SSAT mice. Electron microscopic examination revealed that SSAT mice had an increase in the number and size of mitochondria in WAT compared with Wt mice (Fig. 4A). Furthermore, SSAT mice showed about a twofold increase in the amount of mtDNA in their WAT (Fig. 4B).

Quantitative RT-PCR analyses. In order to verify our Affymetrix results, RT-PCR was used to quantify the expression of genes governing, e.g., mitochondrial metabolic pathways, orphan and nuclear receptors, adipocyte differentiation markers, regulators of glucose uptake and oxidation, and cytokines in WAT. The results were normalized for the expression of β-actin, levels of which were similar in both genotypes. However, we first analyzed the tissue-specific expression of SSAT in WAT, skeletal muscle, and livers of SSAT mice. The expres-

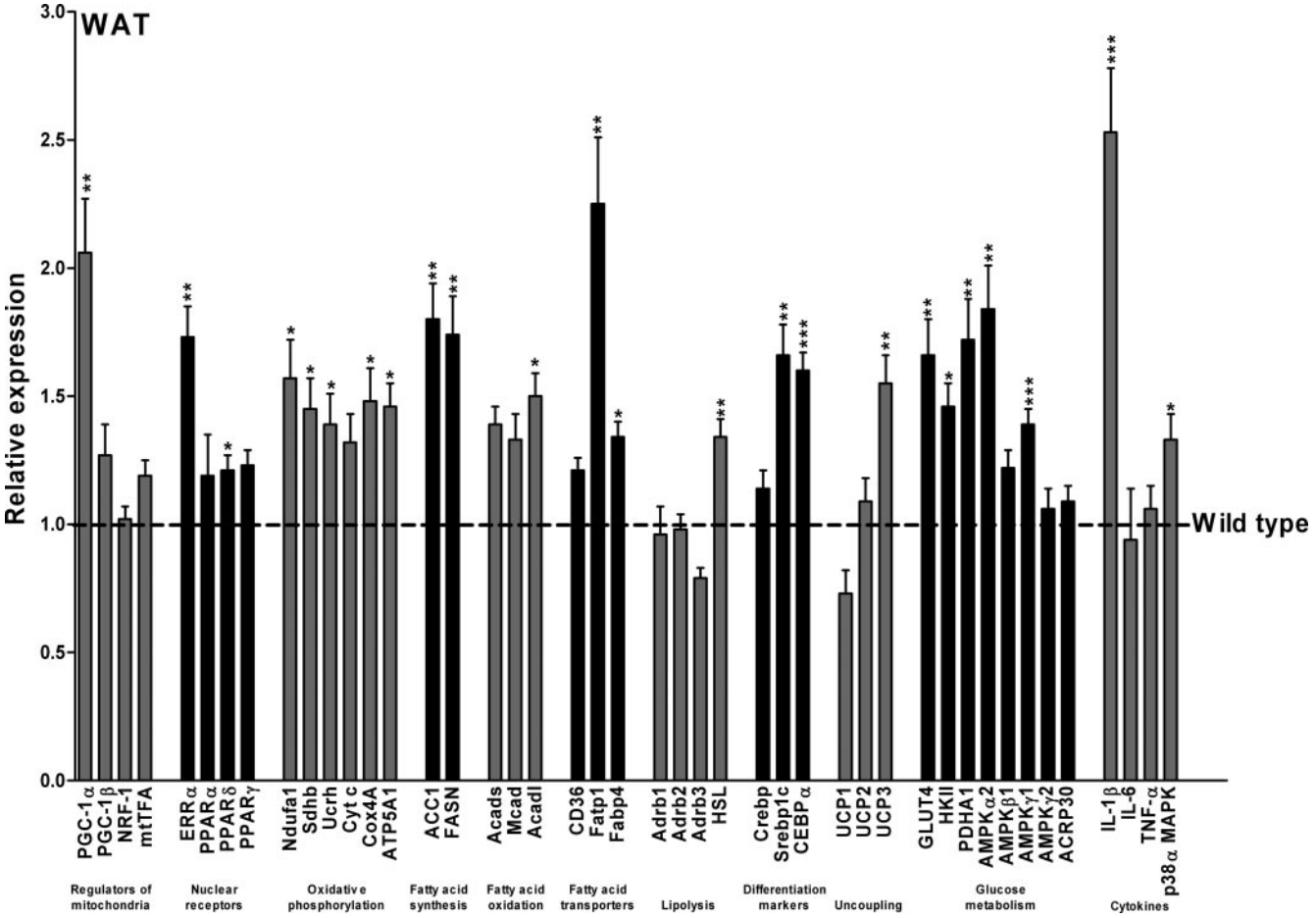

FIG. 5. Selected gene expression profiles in WAT of female SSAT mice compared to those for Wt mice. Data are means ± SEM from eight mice per group. Expression levels of selected genes in fed, 4-month-old female mice were analyzed by quantitative RT-PCR. *, $P < 0.05$; **, $P < 0.01$; ***, $P < 0.001$. NRF-1, nuclear respiratory factor 1; mtTFA, mitochondrial transcription factor A; ERRα, estrogen-related receptor α; Ndufa1, NADH-ubiquinone oxidoreductase MWFE subunit; Sdhb, succinate dehydrogenase iron-sulfur protein; Ucrh, ubiquinol-cytochrome *c* reductase complex; Cyt c, cytochrome *c*; Cox4A, cytochrome *c* oxidase polypeptide IV; ATP5A1, ATP synthase α; ACC1, acetyl-CoA carboxylase 1; FASN, fatty acid synthase; Acads, short-chain acyl-CoA dehydrogenase; Mcad, medium-chain acyl-CoA dehydrogenase; Acadl, long-chain acyl-CoA dehydrogenase; CD36, CD36 antigen/fatty acid translocase; Fatp1, fatty acid transport protein 1; Fabp4, adipocyte-specific fatty acid-binding protein 4; Adrb1, β_1-adenergic receptor; Adrb2, β_2-adenergic receptor; Adrb3, β_3-adenergic receptor; HSL, hormone-sensitive lipase; Crebp, cyclic AMP responsive element binding protein; Srebp1c, sterol regulatory element binding protein 1c; CEBPα, CCAAT/enhancer binding protein α; HKII, hexokinase II; PDHA1, pyruvate dehydrogenase E1 component α subunit; ACRP30, adiponectin; TNF-α, tumor necrosis factor α.

sion of SSAT was markedly upregulated in all tissues studied, but the expression was particularly high in WAT (WAT, 52.5 ± 3.8 times the Wt level [$P < 0.001$]; skeletal muscle, 36.2 ± 2.2 times the Wt level [$P < 0.001$]; liver, 38.7 ± 2.8 times the Wt level [$P < 0.001$]).

As indicated in Fig. 5, the expression of PGC-1α was elevated about twofold in WAT of fed, 4-month-old female SSAT mice compared with that in WAT of Wt mice. In addition, the expression of PGC-1α was also elevated in both female (Tg, 2.72 ± 0.36 times the Wt level [$P = 0.05$]) and male (Tg, 3.45 ± 0.14 times the Wt level [$P < 0.05$]) young, 4-week-old SSAT mice (before hair loss). As Fig. 5 shows, expression levels of PGC-1β and mitochondrial transcription factor A were elevated only slightly in WAT of SSAT mice, and there was no change in expression level of nuclear respiratory factor 1 between the mouse lines. In addition, expression of estrogen-related receptor α followed the expression pattern of PGC-1α in WAT. In SSAT mice, expression levels of of PPARγ and -α were slightly elevated in WAT, whereas expression of PPARδ was significantly increased. Expression levels of six genes related to electron transport complexes (NADH-ubiquinone oxidoreductase MWFE subunit, succinate dehydrogenase iron-sulfur protein, ubiquinol-cytochrome *c* reductase complex, cytochrome *c*, cytochrome *c* oxidase polypeptide IV, and ATP synthase α) were upregulated, indicating increased OXPHOS in SSAT mice.

Expression levels of genes governing fatty acid synthesis, acetyl-coenzyme A (CoA) carboxylase 1, and fatty acid synthase were elevated about twofold, and expression levels of short-chain, medium-chain, and long-chain acyl-CoA dehydrogenases, which catalyze the key reactions in the β-oxidation of fatty acids, were upregulated in WAT. Expression levels of

genes involved in fatty acid uptake and trapping, such as CD36 antigen/fatty acid translocase, fatty acid transport protein 1, and adipocyte-specific fatty acid-binding protein 4, were elevated in SSAT mice. Of the genes involved in the regulation of lipolysis, expression levels for $\beta_{1\text{-}3}$-adenergic receptors in WAT did not differ between SSAT and Wt mice, indicating no change in sensitivity to adrenergic stimuli. In contrast, hormone-sensitive lipase was upregulated in SSAT mice, suggesting that lipolysis may be enhanced in WAT. In addition, transcription factors known to promote adipocyte differentiation (cyclic AMP responsive element binding protein, CCAAT/enhancer binding protein α, and sterol regulatory element binding protein 1c) were upregulated in WAT of SSAT mice. Moreover, of the uncoupling proteins (UCPs), UCP3 expression in WAT was increased in SSAT mice.

Glucose transporter 4 (GLUT4) was upregulated in WAT of SSAT mice 1.7-fold, and expression of hexokinase II, which catalyzes the phosphorylation of glucose to glucose-6-phosphate in WAT and skeletal muscle, was increased in SSAT mice. In addition, expression levels of AMPK isoforms α2 and γ1 were significantly increased but those of isoforms β1 and γ2 were unaltered. Expression of the mitochondrial pyruvate dehydrogenase E1 component α subunit, an indicator of glucose oxidation rate, was enhanced. Expression levels of adiponectin were similar in SSAT and Wt mice.

Of the cytokines, only interleukin 1β (IL-1β) expression was elevated in WAT of SSAT mice. The alpha isoform of p38 MAPK, which controls cellular responses to cytokines and stress, was also upregulated in WAT of SSAT mice.

Characterization of hairless mice. Based on quantitative RT-PCR analyses, the phenotype of our mouse model was apparently due to overexpression of PGC-1α and genes regulated by PGC-1α in WAT. To investigate the possibility that reduced WAT mass and overexpression of PGC-1α in WAT of SSAT mice is due to hairlessness, we examined a mouse line with spontaneous mutation of the hairless gene: hairless MF1-hr mice (55). Four-month-old female hairless hr/hr mice had amounts of perigonadal WAT similar to amounts in normally haired heterozygote hr/+ mice (hr/hr, 0.69% ± 0.11% body weight; hr/+, 0.72% ± 0.23% body weight [*P* was NS]). In contrast, livers (hr/hr, 5.8% ± 0.3% body weight; hr/+, 4.8% ± 0.3% body weight [$P < 0.05$]) and kidneys (hr/hr, 0.70% ± 0.03% body weight; hr/+, 0.56% ± 0.03% body weight [$P < 0.01$]) were significantly enlarged in female hairless mice. The gene expression of PGC-1α was slightly but not significantly reduced (hr/hr, 0.71 ± 0.16 times the hr/+ value [*P* was NS]) in WAT of female hairless mice in comparison with expression in WAT of normally haired heterozygote mice. In addition, fasting glucose (hr/hr, 6.1 ± 0.3 mM; hr/+, 6.2 ± 0.3 mM [*P* was NS]) or insulin (hr/hr, 0.14 ± 0.04 ng/ml; hr/+, 0.26 ± 0.06 ng/ml [*P* was NS]) levels did not differ from those of normally haired heterozygote mice.

Effect of putrescine on gene expression and glucose uptake. Because of the accumulation of putrescine in WAT of SSAT mice, we hypothesized that elevated putrescine levels may induce the expression of PGC-1α directly or indirectly. Factors known to activate PGC-1α expression are cytokines, AMPK, calcium (2), and leptin (65). Cytokines stabilize and activate PGC-1α through direct phosphorylation by phosphorylated p38 MAPK (43). Furthermore, putrescine can directly activate IL-1β production in the human histiocytic lymphoma cell line U937 (58). In SSAT mice, the expression levels of IL-1β and AMPK were increased, suggesting that one or both of them may activate PGC-1α expression in WAT. To test our hypothesis, we gave a high dose of putrescine dihydrochloride (500 mg/kg twice, with a 1-h interval) intraperitoneally to 6-month-old female Wt mice. Animals were sacrificed 2 h after the first injection. Putrescine was administered with or without 25 mg/kg AG, an inhibitor of diamine oxidases, which was given as a pretreatment 2 h before the first putrescine injection. The putrescine treatment caused a massive increase in putrescine concentrations in WAT (data not shown). The putrescine treatment did not induce the gene expression of PGC-1α in WAT. In contrast, it slightly reduced the expression (putrescine, 0.59 ± 0.27 times the control level [*P* was NS]) but the difference was not significant. This result was also verified by measuring protein levels of PGC-1α in WAT (data not shown). In addition, the expression levels of AMPK γ1 (putrescine, 1.20 ± 0.06 times the control level [*P* was NS]) and α2 (putrescine, 0.98 ± 0.12 times the control level [*P* was NS]) isoforms and IL-1β (putrescine, 1.10 ± 0.22 times the control level [*P* was NS]) were similar in putrescine-treated and untreated animals.

In addition, we tested whether putrescine can induce both basal and insulin-stimulated glucose uptake in 3T3-L1 adipocytes. The cells were treated with (i) 1 mM putrescine dihydrochloride with or without 1 mM AG, (ii) 1 mM AG, or (iii) vehicle for 16 h. However, these treatments did not have any significant effect on basal (after 15 min, putrescine, 202 ± 21 cpm/mg protein; putrescine with AG, 209 ± 9 cpm/mg protein; AG, 156 ± 11 cpm/mg protein; vehicle, 155 ± 9 cpm/mg protein [*P* was NS for all]) or insulin-stimulated (after 15 min, putrescine, 2,053 ± 29 cpm/mg protein; putrescine with AG, 2,015 ± 98 cpm/mg protein; AG, 1,594 ± 100 cpm/mg protein; vehicle, 1,740 ± 136 cpm/mg protein [*P* was NS for all]) glucose uptake compared with vehicle treatment. Together, these data suggest that putrescine does not induce the expression of PGC-1α directly or indirectly.

Macrophage content in WAT. WAT contains tissue-resident macrophages and vascular constituents which are located in the stromovascular fraction. Approximately 10% of this fraction includes $CD14^+$ $CD31^+$ macrophages (13). Because SSAT mice had overexpression of IL-1β in WAT, our aim was to determine whether an increased number of macrophages in WAT of SSAT mice caused elevated IL-1β levels, which in turn could induce PGC-1α. Based on immunohistochemical staining, no significant difference in macrophage number in perigonadal fat (Tg, 43 ± 8 mMQ-positive cells/mm^2; Wt, 55 ± 12 mMQ-positive cells/mm^2 [*P* was NS]) or in inguinal fat (Tg, 46 ± 9 mMQ-positive cells/mm^2; Wt, 55 ± 9 mMQ-positive cells/mm^2 [*P* was NS]) was found between SSAT and Wt mice.

Effect of hydrogen peroxide on gene expression of PGC-1α and AMPK isoforms. Accelerated polyamine flux attributable to enhanced polyamine catabolism generates hydrogen peroxide as a by-product of polyamine oxidase and due to the degradation of putrescine by diamine oxidases (22). The findings of Lee et al. (31) indicate that hydrogen peroxide stimulates mitochondrial biogenesis by increasing the expression of nuclear respiratory factor 1 and probably also PGC-1α in human

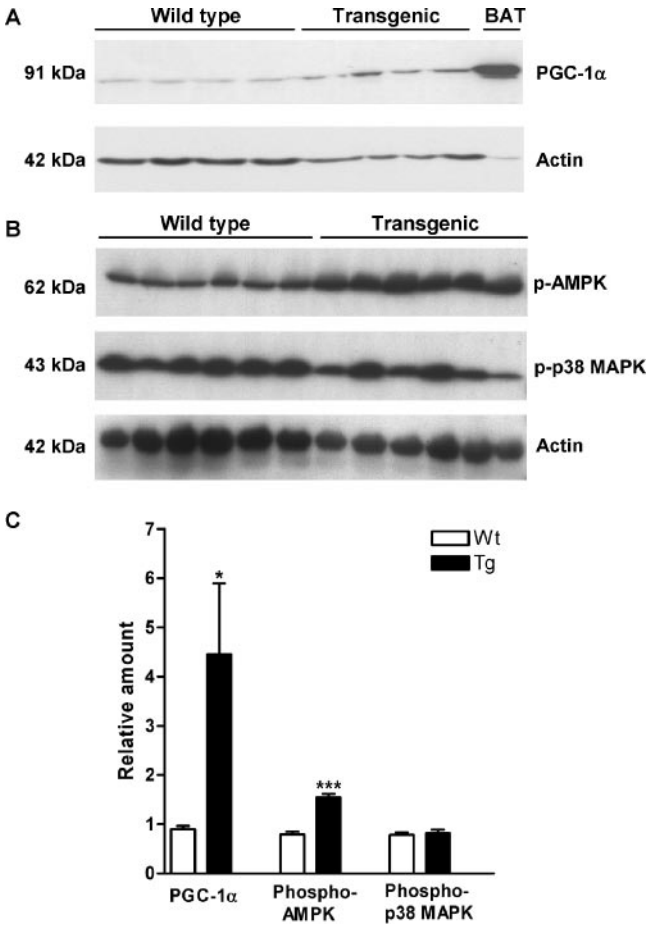

FIG. 6. PGC-1α, phosphorylated AMPK (p-AMPK), and phosphorylated p38 MAPK (p-p38 MAPK) protein levels in WAT of SSAT and Wt mice. (A) PGC-1α levels in WAT of 6-month-old female SSAT and Wt mice, detected with a polyclonal antibody against the carboxyl terminus of PGC-1α (Chemicon International, Inc., Temecula, CA). The bottom panel displays actin levels used for normalization. Actin levels were analyzed using a rabbit polyclonal antibody specific for the carboxyl terminus of actin (Santa Cruz Biotechnology, Inc., Santa Cruz, CA). The BAT sample in the right-most lane was used as a positive control. (B) p-AMPK and p-p38 MAPK levels in WAT of 6-month-old female SSAT and Wt mice, detected with a polyclonal antibody against the phosphorylated α subunit of AMPK(Thr172) (Cell Signaling Technology, Inc., Danvers, MA) and a monoclonal antibody against dually phosphorylated p38 MAPK(Thr180/Tyr182) (Cell Signaling Technology, Inc., Danvers, MA), respectively. The bottom panel displays actin levels used for normalization. Actin levels were analyzed using a rabbit polyclonal antibody specific for the carboxyl terminus of actin (Santa Cruz Biotechnology, Inc., Santa Cruz, CA). (C) Relative PGC-1α, p-AMPK, and p-p38 MAPK protein levels in WAT after normalization in SSAT and Wt mice. Results are expressed as means ± SEM. *, $P < 0.05$; ***, $P < 0.001$.

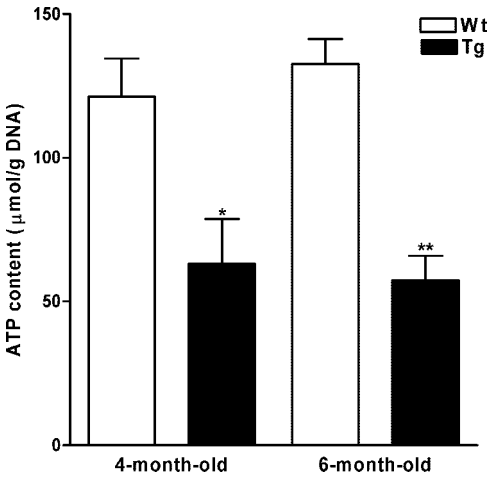

FIG. 7. ATP contents in isolated adipocytes of SSAT and Wt mice. Results are presented as means ± SEM of three separate analyses from pooled adipocytes (two to three animals per group). SSAT and Wt mice used for the experiment were fed, 4- and 6-month-old females. *, $P < 0.05$; **, $P < 0.01$.

lung fibroblasts (MRC-5). In addition, hydrogen peroxide can activate AMPK by reducing the ATP/AMP ratio in NIH 3T3-L1 fibroblasts (9). To investigate whether or not hydrogen peroxide can induce the expression of PGC-1α and/or AMPK in adipocytes, 3T3-L1 adipocytes were exposed to 0, 5, or 10 mU/ml GO, which causes continuous production of hydrogen peroxide in the medium (53). After 16 h of treatment, the expression levels of both PGC-1α (control, 1.00 ± 0.05; GO at 5 mU/ml, 0.75 ± 0.03 times the control level [$P < 0.05$]; GO at 10 mU/ml, 0.46 ± 0.04 times the control level [$P < 0.001$]) and the AMPK γ1 isoform (control, 1.00 ± 0.05; GO at 5 mU/ml, 0.82 ± 0.03 times the control level [$P < 0.05$]; GO at 10 mU/ml, 0.78 ± 0.04 times the control level [$P < 0.05$]) were reduced in a dose-dependent manner. The expression of the AMPK α2 isoform (control, 1.00 ± 0.05; GO at 5 mU/ml, 1.05 ± 0.03 times the control level; GO at 10 mU/ml, 1.12 ± 0.02 times the control level) was unaltered upon the treatment.

PGC-1α, phosphorylated AMPK, and phosphorylated p38 MAPK levels in WAT. Cytokines stabilize and activate PGC-1α through direct phosphorylation by phosphorylated p38 MAPK (43). In addition, oxidative stress increases phosphorylation of both p38 MAPK and AMPK (27). Therefore, protein levels of PGC-1α, phosphorylated p38 MAPK, and AMPK were analyzed. Western blots revealed that the level of 91-kDa full-length PGC-1α protein was elevated 5.0-fold in WAT of SSAT mice (Fig. 6A and C). Phosphorylated p38 MAPK levels were unchanged in WAT of SSAT mice in comparison with levels in WAT of Wt mice (Fig. 6B and C), but the phosphorylated AMPK α subunit was elevated about twofold (Fig. 6B and C). Thus, these results indicate that cytokines and oxidative stress do not induce PGC-1α but that the inducer may be AMPK.

ATP concentrations in isolated adipocytes of SSAT and Wt mice. As AMPK is activated by the reduction of the ATP/AMP ratio (63), we hypothesized that since each polyamine cycle consumes two ATP and two acetyl-CoA molecules (see Fig. 9), enhanced polyamine catabolism may lead to the depletion of the ATP pool in WAT of SSAT mice (22). Low ATP levels may then cause the activation of AMPK, which in turn may induce PGC-1α. Therefore, we measured ATP contents in isolated adipocytes of fed, 4- and 6-month-old female SSAT and Wt mice. We found that 4- and 6-month-old SSAT mice had 48% and 57% lower ATP concentrations, respectively, than Wt mice (Fig. 7).

Activation of polyamine catabolism depletes ATP concentrations in isolated fetal fibroblasts during nutrient deprivation. To test our hypothesis in vitro, isolated fetal fibroblasts

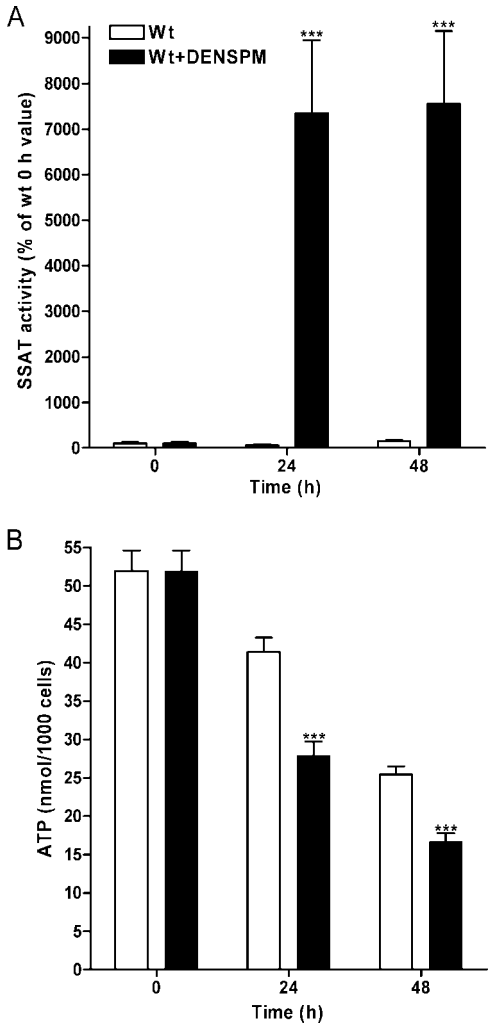

FIG. 8. Effect of activated polyamine catabolism on ATP levels in vitro. (A) SSAT activities and (B) ATP concentrations in Wt fetal fibroblasts with and without DENSPM treatment during nutrient deprivation. Wt cells were grown with or without 10 μM DENSPM for 24 or 48 h in glucose- and sodium pyruvate-free DMEM with glutamine supplemented with 10% dialyzed FBS and 50 μg/ml gentamicin. Each time point represents the mean ± SEM obtained from two independent experiments with triplicate cultures ($n = 6$). ***, $P < 0.001$.

from Wt fetuses were treated with the polyamine analogue DENSPM in order to enhance SSAT activity and therefore activate polyamine catabolism. Fetal fibroblasts overexpressing SSAT were not used since we have shown previously that Tg fetal fibroblasts are sensitive to DENSPM-induced growth inhibition (1). The cells were exposed to nutrient deprivation, since normal cell culture medium contains plenty of energy which can be used to compensate the reduction in ATP levels. DENSPM treatment did not reduce the growth rate of Wt cells in comparison with that of untreated Wt cells. If anything, DENSPM-treated cells grew better after 48 h of nutrient deprivation (data not shown). As indicated in Fig. 8A, DENSPM induced SSAT activity in Wt cells 70- to 75-fold at 24 h and 48 h, respectively. In addition, DENSPM treatment significantly reduced polyamine pools at 24 h (putrescine DENSPM, 0 ± 0 pmol/μg protein; control, 1.67 ± 0.01 pmol/μg protein [$P < 0.001$]) (spermidine DENSPM, 1.18 ± 0.04 pmol/μg protein; control, 12.24 ± 0.20 pmol/μg protein [$P < 0.001$]) (spermine DENSPM, 1.42 ± 0.03 pmol/μg protein; control, 3.35 ± 0.07 pmol/μg protein [$P < 0.001$]) and 48 h (putrescine DENSPM, 0 ± 0 pmol/μg protein; control, 2.42 ± 0.17 pmol/μg protein [$P < 0.001$]) (spermidine DENSPM, 0.48 ± 0.02 pmol/μg protein; control, 14.58 ± 0.81 pmol/μg protein [$P < 0.001$]) (spermine DENSPM, 0.92 ± 0.01 pmol/μg protein; control, 4.00 ± 0.13 pmol/μg protein [$P < 0.001$]). As Fig. 8B shows, nutrient deprivation reduced ATP pools in a time-dependent manner in untreated and DENSPM-treated cells, as expected. However, DENSPM-treated Wt fetal fibroblasts had significantly lower ATP levels than untreated Wt cells at 24 h and 48 h (Fig. 8B), suggesting that activated polyamine catabolism depletes ATP also in vitro.

Inhibition of the rate of polyamine flux reversed the phenotype of SSAT mice. To investigate whether a reduction in the rate of the polyamine cycle will reverse the phenotype of SSAT mice, we used a specific inhibitor of ODC, DFMO, to block the putrescine supply from compensatorily increased biosynthesis. We added 0.5% DFMO for 2, 4, or 5 weeks to the drinking water of SSAT and Wt mice after weaning, when SSAT mice start to lose their hair. The treatment clearly slowed down the polyamine cycle in SSAT mice, as putrescine levels were reduced in WAT by about 55% after 2 weeks and about 70% after 5 weeks in SSAT mice (Table 3). In addition, a 4-week treatment increased ATP levels about 60% in an isolated adipocyte pool of SSAT mice in comparison with levels for untreated animals (Tg untreated mice, 47.5 μmol/g; Tg mice treated with DFMO, 75.7 μmol/g). The DFMO treatment did not have any effect on body composition in Wt mice, but in SSAT mice it caused about a twofold increase in the amount of perigonadal WAT after 2 weeks and about a 2.3-fold increase after 5 weeks compared with amounts for untreated SSAT mice (Table 3). Gene expression profiles were also subsequently monitored after the 2-week treatment, when there was no visible hair regrowth (42). Interestingly, the DFMO treatment reduced the expression levels of the AMPK γ1 isoform and PCG-1α to near-Wt levels (Table 4). Similarly, the expression levels of all genes induced by PGC-1α were significantly reduced in response to the treatment. In contrast, the expression of IL-1β was practically unaltered by the DFMO treatment (Table 4). Thus, the DFMO treatment was able to reverse the phenotype of SSAT mice (Table 4).

DISCUSSION

The main findings of this study were that Tg mice overexpressing SSAT (41) had severely reduced WAT, increased basal metabolic rate, improved glucose tolerance and insulin sensitivity, low accumulation of TG in liver and skeletal muscle, and increased expression of OXPHOS genes, coordinated by the increased expression of PGC-1α and AMPK in WAT. These changes were induced by accelerated polyamine flux due to enhanced polyamine catabolism and the consumption of ATP. This is a novel mechanism for reduced fat mass and improved glucose tolerance and indicates that polyamine catabolism can regulate energy and glucose metabolism.

WAT was the main tissue affected by enhanced polyamine catabolism in SSAT mice since SSAT activity was highest in

TABLE 3. Effect of DFMO treatment on weight, amount of perigonadal WAT, and polyamine concentration of WAT in female and male SSAT and Wt mice[a]

Sample time point and mouse group	Wt (g)	Peri WAT (mg)	Peri WAT (% of body wt)	Polyamine pool (pmol/μg DNA)			
				Putrescine	N^1-acetyl-spermidine	Spermidine	Spermine
2 Wk							
Wt	16.8 ± 0.5	162 ± 16	0.94 ± 0.07	6 ± 1	ND	131 ± 15	56 ± 7
Wt with DFMO	16.8 ± 0.7	195 ± 29	1.07 ± 0.12	3 ± 1	ND	104 ± 11	51 ± 8
SSAT	15.4 ± 0.5	50 ± 5†	0.34 ± 0.03†	302 ± 51†††	8 ± 2†	117 ± 19	41 ± 9
SSAT with DFMO	15.5 ± 0.5	110 ± 12†	0.69 ± 0.03†*	151 ± 11†††***	8 ± 3†	96 ± 6	39 ± 3
5 Wk							
Wt	21.7 ± 0.9	460 ± 91	2.07 ± 0.35	17 ± 3	ND	202 ± 27	90 ± 12
Wt with DFMO	21.8 ± 1.6	468 ± 112	1.98 ± 0.36	19 ± 4	ND	166 ± 17	71 ± 9
SSAT	20.6 ± 0.9	155 ± 39†	0.72 ± 0.17†	506 ± 119†††	13 ± 3†	145 ± 37	50 ± 13†
SSAT with DFMO	21.9 ± 0.9	364 ± 68	1.62 ± 0.25	153 ± 13†††***	6 ± 4	119 ± 14†	37 ± 6††

[a] Results are expressed as means ± SEM from 4 to 19 mice per genotype. Values marked with an asterisk(s) are significantly different from the baseline level. *, $P < 0.05$; ***, $P < 0.001$. Values marked with a dagger(s) are significantly different compared to levels for Wt mice. †, $P < 0.05$; ††, $P < 0.01$; †††, $P < 0.001$. Peri WAT, perigonadal WAT; ND, not detected.

this tissue. Adipocytes of SSAT mice were smaller than Wt cells, but the total number of adipocytes was similar to that for Wt mice. The number of mitochondria in adipocytes was increased, a typical feature of BAT, but no brown fat-like multilocular cells were detected. Polyamines, especially spermidine and putrescine, are shown to be needed for the differentiation of 3T3-L1 fibroblasts to adipocytes (4). In WAT of SSAT mice, spermidine levels remained unchanged and putrescine levels were substantially increased. Furthermore, expression levels of transcription factors promoting adipocyte differentiation were upregulated in WAT of SSAT mice, suggesting that adipocyte differentiation in SSAT mice is likely to be normal.

The expression of fatty acid transporters was elevated, excluding the possibility that fatty acid uptake into the adipocytes is impaired. Therefore, our results indicate that the main reason for reduced fat mass was an increased metabolic rate in SSAT mice. As these mice were less active than Wt mice, the increased metabolic rate was apparently not due to increased physical activity. In agreement with an increased basal metabolic rate, SSAT mice were hyperphagic, which could result from reduced leptin levels (46). Importantly, SSAT mice had reduced perigonadal fat mass, fasting insulin levels, increased basal metabolic rate, and elevated expression of PGC-1α in WAT even before hair loss. In addition, no significant changes in perigonadal fat mass, fasting glucose or insulin levels, or expression of PGC-1α were found in WAT of hairless hr/hr mice compared with levels in WAT of normally haired heterozygote hr/+ mice. Therefore, the phenotype of SSAT mice cannot be secondary to the hairlessness.

SSAT mice exhibited improved glucose tolerance and increased insulin sensitivity, and these mice had a markedly reduced accumulation of TG in liver and skeletal muscle, consistent with enhanced insulin action. Accordingly, the expression levels of GLUT4, hexokinase II, and the pyruvate dehydrogenase E1 component α subunit, apparently induced by the increased expression of PGC-1α and AMPK, were increased in WAT, reflecting increased rates of glucose uptake and glucose oxidation. Therefore, increased insulin sensitivity was not a consequence of reduced fat mass or tissue TGs, although the correlation between insulin sensitivity and leanness (18) and reduced intracellular TG content (29) is well established.

TABLE 4. Effect of 2 weeks of DFMO treatment on gene expression profiles in perigonadal WAT of female SSAT and Wt mice

Gene designation	Gene description	Gene expression level[a] for SSAT mice		*P* value for effect of treatment
		Without DFMO	With DFMO	
AMPKα2	5′-AMP-activated protein kinase, alpha-2 subunit	1.47 ± 0.10	1.06 ± 0.19	NS
AMPKγ1	5′-AMP-activated protein kinase, gamma-1 subunit	1.85 ± 0.18***	0.86 ± 0.13	<0.001
PGC-1α	Peroxisome proliferator-activated receptor gamma coactivator 1α	2.02 ± 0.53	1.15 ± 0.20	NS
ERRα	Estrogen-related receptor alpha	2.31 ± 0.33**	1.17 ± 0.49	<0.01
Ndufa1	NADH-ubiquinone oxidoreductase MWFE subunit	1.57 ± 0.10***	1.01 ± 0.19	<0.01
Sdhb	Succinate dehydrogenase iron-sulfur protein	2.75 ± 0.19**	1.67 ± 0.37	<0.05
Cox4A	Cytochrome *c* oxidase polypeptide IV	2.43 ± 0.12**	1.58 ± 0.38	NS
ATP5A1	ATP synthase alpha	2.47 ± 0.04***	1.61 ± 0.18	<0.05
PPARγ	Peroxisome proliferator-activated receptor gamma	2.38 ± 0.20***	1.03 ± 0.15	<0.01
UCP3	Uncoupling protein 3	2.41 ± 0.15***	0.83 ± 0.24	<0.001
GLUT4	Glucose transporter 4	3.61 ± 0.51***	1.47 ± 0.17	<0.001
IL-1β	Interleukin 1 beta	1.74 ± 0.34	1.49 ± 0.11	NS

[a] Gene expression levels indicate the increase (*n*-fold) above the Wt level. Results are expressed as means ± SEM from three to four animals per group. Values marked with an asterisk(s) are significantly different from levels for Wt mice. **, $P < 0.01$; ***, $P < 0.001$.

The increased metabolic rate in SSAT mice is best explained by the overexpression of PGC-1α and AMPK in WAT. First, there was an abundance of mitochondria in WAT of SSAT mice, most probably induced by PGC-1α (49). Second, SSAT mice had enhanced palmitate oxidation in isolated adipocytes, apparently activated by PGC-1α and AMPK (23, 61). In agreement with enhanced fatty acid oxidation, the expression levels of PPARδ and estrogen-related receptor α, genes governing the regulation of fatty acid oxidation, were upregulated and RQ levels were lower after fasting in the active state. Third, the expression levels of genes involved in OXPHOS were increased in WAT, most likely coordinated by PGC-1α (36), indicating increased OXPHOS in WAT of SSAT mice. Fourth, PGC-1α and AMPK increase uncoupling (45, 54) and accordingly UCP3 was upregulated in WAT of SSAT mice. Overall, the characteristics of SSAT mice resemble those of mice overexpressing PGC-1α in WAT (7, 59). These mice also have an increased metabolic rate, reduced fat pads, increased uncoupling and insulin sensitivity, and protection from diet-induced obesity.

In order to determine mechanisms leading to the phenotype of SSAT mice, we first excluded the possibility that the upregulation of PGC-1α or its inducers (AMPK and IL-1β) in WAT of SSAT mice could be related to the enhanced accumulation of putrescine. Indeed, we did not notice any induction of the expression of PGC-1α, AMPK isoforms, or IL-1β in putrescine-treated mice or an increase in glucose uptake in 3T3-L1 adipocytes by putrescine. Furthermore, we observed that the production of hydrogen peroxide in 3T3-L1 adipocytes reduced the expression of PGC-1α and the AMPK γ1 isoform in a dose-dependent manner. Therefore, the possibility that hydrogen peroxide induced overexpression of PGC-1α or AMPK can be excluded.

Oxidative stress caused by hydrogen peroxide mediates its effects through both p38 MAPK and AMPK (27). Moreover, cytokines stabilize and activate PGC-1α through phosphorylation by phosphorylated p38 MAPK (43). Since phosphorylated p38 MAPK was unaltered in WAT of SSAT mice, our results together with the unaltered macrophage number in WAT suggest that neither oxidative stress (H_2O_2) nor cytokines (IL-1β) induced PGC-1α. Therefore, the increased amount of phosphorylated AMPK in WAT of SSAT mice suggests that the most plausible inducer of PGC-1α was AMPK.

We propose a mechanism to explain how SSAT overexpression leads to the phenotype of SSAT mice (Fig. 9). Since each polyamine cycle consumes four ATP equivalents (two ATP and two acetyl-CoA), activated polyamine catabolism results in the depletion of the ATP pool in adipocytes of SSAT mice. Consequently, the high AMP/ATP ratio activates AMPK, which in turn activates PGC-1α. Our hypothesis is supported by in vitro data showing that activated polyamine catabolism depleted ATP levels in DENSPM-treated Wt fibroblasts compared with levels in untreated Wt cells. In addition, the reduction in the rate of the polyamine cycle due to the administration of DFMO, a specific inhibitor of ODC, increased ATP levels in adipocytes and reversed the phenotype of SSAT mice. This gives further support to our hypothesis that the polyamine cycle can be considered a futile cycle wasting ATP.

We have demonstrated that a consequence of the accelerated polyamine flux due to enhanced polyamine catabolism is the depletion of ATP and possibly of acetyl-CoA. In fact, when this paper was in review, Jell et al. (22a) reported similar and complementary results, including the observation that pools of acetyl-CoA and malonyl-CoA were markedly reduced in WAT of SSAT mice. The depletion of ATP can induce AMPK and PGC-1α expression in WAT and lead to the reduction in fat mass, the increased basal metabolic rate and insulin sensitivity, and the overexpression of the OXPHOS pathway. Therefore, our results suggest that polyamine catabolism plays an important role in the regulation of energy and glucose metabolism. SSAT is a highly inducible enzyme (6); thus, compounds capable of inducing SSAT activity could be useful tools for activating polyamine catabolism in WAT. The involvement of polyamine catabolism in the regulation of energy and glucose metabolism may offer a novel target for drug development for obesity and type 2 diabetes.

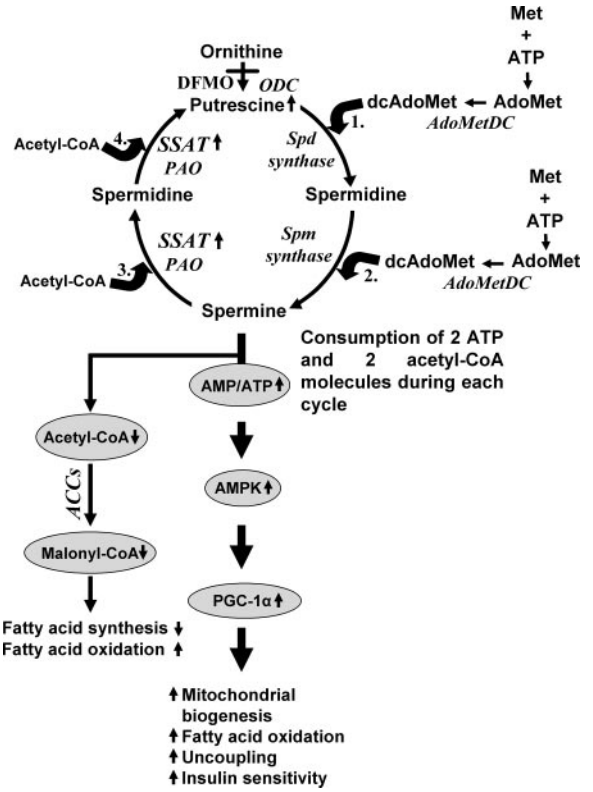

FIG. 9. Proposed molecular mechanism leading to the phenotype of SSAT mice. Based on the data presented, it is hypothesized that the accelerated polyamine flux caused by enhanced polyamine catabolism in WAT leads to the high ATP consumption and the high AMP/ATP ratio which stimulates AMPK. This in turn induces the expression of PGC-1α, resulting in increased mitochondrial biogenesis, fatty acid oxidation, uncoupling, and insulin sensitivity. The enhanced polyamine catabolism also depletes the SSAT cofactor acetyl-CoA pool and therefore may cause impaired generation of malonyl-CoA by acetyl-CoA carboxylases (ACCs), leading to reduced fatty acid synthesis and increased fatty acid oxidation. DFMO is an inhibitor of ODC, and it reduces the biosynthesis of putrescine and therefore the rate of the polyamine cycle. PAO, polyamine oxidase; Spd, spermidine; Spm, spermine; Met, methionine; AdoMet, *S*-adenosylmethionine; Ado MetDC, *S*-adenosylmethionine decarboxylase; dcAdoMet, decarboxylated *S*-adenosylmethionine.

ACKNOWLEDGMENTS

This work was supported by grants to E.P. from the Finnish Cultural Foundation of Northern Savo, the Finnish Cultural Foundation, the Diabetes Research Foundation, the Kuopio University Foundation, and the Research and Science Foundation of Farmos and to M.L. from the Academy of Finland and the European Union (LSHM-CT-2004-512013).

We are grateful to Mia Urjansson, Aino Johansson, Anne Karppinen, Arja Korhonen, Tuula Reponen, Sisko Juutinen, Marita Heikkinen, Riikka Frilander-Keinänen, Alpo Pelttari, Virpi Miettinen, Marika Kamps, Teija Oinonen, Rauni Tapaninen, and Eveliina Kiriloff for their excellent technical assistance. In addition, we thank Miina Miller and Krista Haapalainen at the Microarray and Bioinformatics Centre for Biotechnology, Turku, Finland, for Affymetrix analyses. We also wish to thank Tuomo Keinänen for his advice and helpful discussions about polyamine metabolism.

REFERENCES

1. **Alhonen, L., A. Karppinen, M. Uusi-Oukari, S. Vujcic, V. P. Korhonen, M. Halmekytö, D. L. Kramer, R. Hines, J. Jänne, and C. W. Porter.** 1998. Correlation of polyamine and growth responses to N1,N11-diethylnorspermine in primary fetal fibroblasts derived from transgenic mice overexpressing spermidine/spermine N1-acetyltransferase. J. Biol. Chem. **273:**1964–1969.
2. **Attie, A. D., and C. M. Kendziorski.** 2003. PGC-1alpha at the crossroads of type 2 diabetes. Nat. Genet. **34:**244–245.
3. **Bernacki, R. J., E. J. Oberman, K. E. Seweryniak, A. Atwood, R. J. Bergeron, and C. W. Porter.** 1995. Preclinical antitumor efficacy of the polyamine analogue N1, N11-diethylnorspermine administered by multiple injection or continuous infusion. Clin. Cancer Res. **1:**847–857.
4. **Bethell, D. R., and A. E. Pegg.** 1981. Polyamines are needed for the differentiation of 3T3-L1 fibroblasts into adipose cells. Biochem. Biophys. Res. Commun. **102:**272–278.
5. **Birnbaum, M. J.** 2005. Activating AMP-activated protein kinase without AMP. Mol. Cell **19:**289–290.
6. **Casero, R. A., Jr., and A. E. Pegg.** 1993. Spermidine/spermine N1-acetyltransferase—the turning point in polyamine metabolism. FASEB J. **7:**653–661.
7. **Cederberg, A., L. M. Grønning, B. Ahren, K. Tasken, P. Carlsson, and S. Enerbäck.** 2001. FOXC2 is a winged helix gene that counteracts obesity, hypertriglyceridemia, and diet-induced insulin resistance. Cell **106:**563–573.
8. **Cheung, P. C., I. P. Salt, S. P. Davies, D. G. Hardie, and D. Carling.** 2000. Characterization of AMP-activated protein kinase gamma-subunit isoforms and their role in AMP binding. Biochem. J. **346:**659–669.
9. **Choi, S. L., S. J. Kim, K. T. Lee, J. Kim, J. Mu, M. J. Birnbaum, S. Soo Kim, and J. Ha.** 2001. The regulation of AMP-activated protein kinase by H_2O_2. Biochem. Biophys. Res. Commun. **287:**92–97.
10. **Chomczynski, P., and N. Sacchi.** 1987. Single-step method of RNA isolation by acid guanidium thiocyanate-phenol-chloroform extraction. Anal. Biochem. **167:**156–159.
11. **Dahlquist, K. D., N. Salomonis, K. Vranizan, S. C. Lawlor, and B. R. Conklin.** 2002. GenMAPP, a new tool for viewing and analyzing microarray data on biological pathways. Nat. Genet. **31:**19–20.
12. **Doniger, S. W., N. Salomonis, K. D. Dahlquist, K. Vranizan, S. C. Lawlor, and B. R. Conklin.** 2003. MAPPFinder: using gene ontology and GenMAPP to create a global gene-expression profile from microarray data. Genome Biol. **4:**R7.
13. **Fantuzzi, G.** 2005. Adipose tissue, adipokines, and inflammation. J. Allergy Clin. Immunol. **115:**911–919.
14. **Giles, K. W., and A. Myers.** 1964. The role of nucleic acids in the growth of the hypocotyl of lupinus albus under varying light and dark regimes. Biochim. Biophys. Acta **87:**460–477.
15. **Hammarstedt, A., P. A. Jansson, C. Wesslau, X. Yang, and U. Smith.** 2003. Reduced expression of PGC-1 and insulin-signaling molecules in adipose tissue is associated with insulin resistance. Biochem. Biophys. Res. Commun. **301:**578–582.
16. **Hardie, D. G.** 2004. The AMP-activated protein kinase pathway—new players upstream and downstream. J. Cell Sci. **117:**5479–5487.
17. **Harrington, T. A., E. L. Thomas, N. Modi, G. Frost, G. A. Coutts, and J. D. Bell.** 2002. Fast and reproducible method for the direct quantitation of adipose tissue in newborn infants. Lipids **37:**95–100.
18. **Heilbronn, L., S. R. Smith, and E. Ravussin.** 2004. Failure of fat cell proliferation, mitochondrial function and fat oxidation results in ectopic fat storage, insulin resistance and type II diabetes mellitus. Int. J. Obes. Relat. Metab. Disord. **28:**S12–S21.
19. **Hohtola, E., R. Hissa, A. Pyörnilä, H. Rintamäki, and S. Saarela.** 1991. Nocturnal hypothermia in fasting Japanese quail: the effect of ambient temperature. Physiol. Behav. **49:**563–567.
20. **Hyvönen, T., T. A. Keinänen, A. R. Khomutov, R. M. Khomutov, and T. O. Eloranta.** 1992. Monitoring of the uptake and metabolism of aminooxy analogues of polyamines in cultured cells by high-performance liquid chromatography. J. Chromatogr. **574:**17–21.
21. **Jänne, J., L. Alhonen, M. Pietilä, and T. A. Keinänen.** 2004. Genetic approaches to the cellular functions of polyamines in mammals. Eur. J. Biochem. **271:**877–894.
22. **Jänne, J., L. Alhonen, M. Pietilä, T. A. Keinänen, A. Uimari, M. T. Hyvönen, E. Pirinen, and A. Järvinen.** 2006. Genetic manipulation of polyamine catabolism in rodents. J. Biochem. (Tokyo) **139:**155–160.

22a. **Jell, J., S. Merali, M. L. Hensen, R. Mazurchuk, J. A. Spernyak, P. Diegelman, N. D. Kisiel, C. Barrero, K. K. Deeb, L. Alhonen, M. S. Patel, and C. W. Porter.** 2007. Genetically altered expression of spermidine/spermine N^1-acetyltransferase affects fat metabolism in mice via acetyl-CoA. J. Biol. Chem. **282:**8404–8413.

23. **Kahn, B. B., T. Alquier, D. Carling, and D. G. Hardie.** 2005. AMP-activated protein kinase: ancient energy gauge provides clues to modern understanding of metabolism. Cell Metab. **1:**15–25.
24. **Kee, K., B. A. Foster, S. Merali, D. L. Kramer, M. L. Hensen, P. Diegelman, N. Kisiel, S. Vujcic, R. V. Mazurchuk, and C. W. Porter.** 2004. Activated polyamine catabolism depletes acetyl-CoA pools and suppresses prostate tumor growth in TRAMP mice. J. Biol. Chem. **279:**40076–40083.
25. **Kelly, M., C. Keller, P. R. Avilucea, P. Keller, Z. Luo, X. Xiang, M. Giralt, J. Hidalgo, A. K. Saha, B. K. Pedersen, and N. B. Ruderman.** 2004. AMPK activity is diminished in tissues of IL-6 knockout mice: the effect of exercise. Biochem. Biophys. Res. Commun. **320:**449–454.
26. **Kiens, B., and E. A. Richter.** 1996. Types of carbohydrate in an ordinary diet affect insulin action and muscle substrates in humans. Am. J. Clin. Nutr. **63:**47–53.
27. **Kim, J. S., V. Saengsirisuwan, J. A. Sloniger, M. K. Teachey, and E. J. Henriksen.** 2006. Oxidant stress and skeletal muscle glucose transport: roles of insulin signaling and p38 MAPK. Free Radic. Biol. Med. **41:**818–824.
28. **Krotkiewski, M., P. Björntorp, L. Sjöström, and U. Smith.** 1983. Impact of obesity on metabolism in men and women. Importance of regional adipose tissue distribution. J. Clin. Investig. **72:**1150–1162.
29. **Krssak, M., K. Falk Petersen, A. Dresner, L. DiPietro, S. M. Vogel, D. L. Rothman, M. Roden, and G. I. Shulman.** 1999. Intramyocellular lipid concentrations are correlated with insulin sensitivity in humans: a 1H NMR spectroscopy study. Diabetologia **42:**113–116.
30. **Laakso, M.** 2001. Insulin resistance and its impact on the approach to therapy of type 2 diabetes. Int. J. Clin. Pract. Suppl. **121:**8–12.
31. **Lee, H. C., P. H. Yin, C. W. Chi, and Y. H. Wei.** 2002. Increase in mitochondrial mass in human fibroblasts under oxidative stress and during replicative cell senescence. J. Biomed. Sci. **9:**517–526.
32. **Leppänen, P., J. S. Luoma, M. H. Hofker, L. M. Havekes, and S. Ylä-Herttuala.** 1998. Characterization of atherosclerotic lesions in apo E3-leiden transgenic mice. Atherosclerosis **136:**147–152.
33. **Lockwood, D. H., and L. E. East.** 1974. Studies of the insulin-like actions of polyamines on lipid and glucose metabolism in adipose tissue cells. J. Biol. Chem. **249:**7717–7722.
34. **McLean, J. A., and G. Tobin.** 1990. Animal and human calorimetry. Cambridge University Press, Cambridge, United Kingdom.
35. **Michael, L. F., Z. Wu, R. B. Cheatham, P. Puigserver, G. Adelmant, J. J. Lehman, D. P. Kelly, and B. M. Spiegelman.** 2001. Restoration of insulin-sensitive glucose transporter (GLUT4) gene expression in muscle cells by the transcriptional coactivator PGC-1. Proc. Natl. Acad. Sci. USA **98:**3820–3825.
36. **Mootha, V. K., C. M. Lindgren, K. F. Eriksson, A. Subramanian, S. Sihag, J. Lehar, P. Puigserver, E. Carlsson, M. Ridderstrale, E. Laurila, N. Houstis, M. J. Daly, N. Patterson, J. P. Mesirov, T. R. Golub, P. Tamayo, B. Spiegelman, E. S. Lander, J. N. Hirschhorn, D. Altshuler, and L. C. Groop.** 2003. PGC-1alpha-responsive genes involved in oxidative phosphorylation are coordinately downregulated in human diabetes. Nat. Genet. **34:**267–273.
37. **Osmundsen, H.** 1981. Spectrophotometric procedure for measuring mitochondrial beta-oxidation. Methods Enzymol. **72:**306–314.
38. **Pallotti, F., and G. Lenaz.** 2001. Isolation and subfractionation of mitochondria from animal cells and tissue culture lines. Methods Cell. Biol. **65:**1–35.
39. **Passonneau, J. V., and O. H. Lowry.** 1993. Enzymatic analysis: a practical guide. Humana Press, Ottawa, Ontario, Canada.
40. **Patti, M. E., A. J. Butte, S. Crunkhorn, K. Cusi, R. Berria, S. Kashyap, Y. Miyazaki, I. Kohane, M. Costello, R. Saccone, E. J. Landaker, A. B. Goldfine, E. Mun, R. DeFronzo, J. Finlayson, C. R. Kahn, and L. J. Mandarino.** 2003. Coordinated reduction of genes of oxidative metabolism in humans with insulin resistance and diabetes: potential role of PGC1 and NRF1. Proc. Natl. Acad. Sci. USA **100:**8466–8471.
41. **Pietilä, M., L. Alhonen, M. Halmekytö, P. Kanter, J. Jänne, and C. W. Porter.** 1997. Activation of polyamine catabolism profoundly alters tissue polyamine pools and affects hair growth and female fertility in transgenic mice overexpressing spermidine/spermine N1-acetyltransferase. J. Biol. Chem. **272:**18746–18751.
42. **Pietilä, M., E. Pirinen, S. Keskitalo, S. Juutinen, S. Pasonen-Seppänen, T. Keinänen, L. Alhonen, and J. Jänne.** 2005. Disturbed keratinocyte differentiation in transgenic mice and organotypic keratinocyte cultures as a result of spermidine/spermine N-acetyltransferase overexpression. J. Investig. Dermatol. **124:**596–601.

43. **Puigserver, P., J. Rhee, J. Lin, Z. Wu, J. C. Yoon, C. Y. Zhang, S. Krauss, V. K. Mootha, B. B. Lowell, and B. M. Spiegelman.** 2001. Cytokine stimulation of energy expenditure through p38 MAP kinase activation of PPARgamma coactivator-1. Mol. Cell **8:**971–982.
44. **Puigserver, P., and B. M. Spiegelman.** 2003. Peroxisome proliferator-activated receptor-gamma coactivator 1 alpha (PGC-1 alpha): transcriptional coactivator and metabolic regulator. Endocr. Rev. **24:**78–90.
45. **Puigserver, P., Z. Wu, C. W. Park, R. Graves, M. Wright, and B. M. Spiegelman.** 1998. A cold-inducible coactivator of nuclear receptors linked to adaptive thermogenesis. Cell **92:**829–839.
46. **Robinson, S. W., D. M. Dinulescu, and R. D. Cone.** 2000. Genetic models of obesity and energy balance in the mouse. Annu. Rev. Genet. **34:**687–745.
47. **Rodbell, M.** 1964. Metabolism of isolated fat cells. I. Effects of hormones on glucose metabolism and lipolysis. J. Biol. Chem. **239:**375–380.
48. **Salt, I., J. W. Celler, S. A. Hawley, A. Prescott, A. Woods, D. Carling, and D. G. Hardie.** 1998. AMP-activated protein kinase: greater AMP dependence, and preferential nuclear localization, of complexes containing the alpha2 isoform. Biochem. J. **334:**177–187.
49. **Scarpulla, R. C.** 2002. Nuclear activators and coactivators in mammalian mitochondrial biogenesis. Biochim. Biophys. Acta **1576:**1–14.
50. **Semple, R. K., V. C. Crowley, C. P. Sewter, M. Laudes, C. Christodoulides, R. V. Considine, A. Vidal-Puig, and S. O'Rahilly.** 2004. Expression of the thermogenic nuclear hormone receptor coactivator PGC-1alpha is reduced in the adipose tissue of morbidly obese subjects. Int. J. Obes. Relat. Metab. Disord. **28:**176–179.
51. **Shelepov, V. P., V. A. Chekulaev, and G. R. Pasha-Zade.** 1990. Effect of putrescine on carbohydrate and lipid metabolism in rats. Biomed. Sci. **1:**591–596.
52. **Smith, U., L. Sjöström, and P. Björnstorp.** 1972. Comparison of two methods for determining human adipose cell size. J. Lipid Res. **13:**822–824.
53. **Soares, A. F., M. Guichardant, D. Cozzone, N. Bernoud-Hubac, N. Bouzaidi-Tiali, M. Lagarde, and A. Geloen.** 2005. Effects of oxidative stress on adiponectin secretion and lactate production in 3T3-L1 adipocytes. Free Radic. Biol. Med. **38:**882–889.
54. **Stoppani, J., A. L. Hildebrandt, K. Sakamoto, D. Cameron-Smith, L. J. Goodyear, and P. D. Neufer.** 2002. AMP-activated protein kinase activates transcription of the UCP3 and HKII genes in rat skeletal muscle. Am. J. Physiol. Endocrinol. Metab. **283:**E1239–E1248.
55. **Stoye, J. P., S. Fenner, G. E. Greenoak, C. Moran, and J. M. Coffin.** 1988. Role of endogenous retroviruses as mutagens: the hairless mutation of mice. Cell **54:**383–391.
56. **St.-Pierre, J., J. Lin, S. Krauss, P. T. Tarr, R. Yang, C. B. Newgard, and B. M. Spiegelman.** 2003. Bioenergetic analysis of peroxisome proliferator-activated receptor gamma coactivators 1alpha and 1beta (PGC-1alpha and PGC-1beta) in muscle cells. J. Biol. Chem. **278:**26597–26603.
57. **Student, A. K., R. Y. Hsu, and M. D. Lane.** 1980. Induction of fatty acid synthetase synthesis in differentiating 3T3-L1 preadipocytes. J. Biol. Chem. **255:**4745–4750.
58. **Tahara, H., S. Otani, I. Matsui-Yuasa, H. Koyama, Y. Nishizawa, S. Morisawa, and H. Morii.** 1991. Role of putrescine in interleukin 1 beta production in human histiocytic lymphoma cell line U937. J. Cell. Physiol. **147:**199–207.
59. **Tsukiyama-Kohara, K., F. Poulin, M. Kohara, C. T. DeMaria, A. Cheng, Z. Wu, A. C. Gingras, A. Katsume, M. Elchebly, B. M. Spiegelman, M. E. Harper, M. L. Tremblay, and N. Sonenberg.** 2001. Adipose tissue reduction in mice lacking the translational inhibitor 4E-BP1. Nat. Med. **7:**1128–1132.
60. **Ushmorov, A., V. Hack, and W. Droge.** 1999. Differential reconstitution of mitochondrial respiratory chain activity and plasma redox state by cysteine and ornithine in a model of cancer cachexia. Cancer Res. **59:**3527–3534.
61. **Vega, R. B., J. M. Huss, and D. P. Kelly.** 2000. The coactivator PGC-1 cooperates with peroxisome proliferator-activated receptor alpha in transcriptional control of nuclear genes encoding mitochondrial fatty acid oxidation enzymes. Mol. Cell. Biol. **20:**1868–1876.
62. **Wieland, O.** 1974. Glyserol assay, p. 1404–1406. *In* H. V. Bergmeyer (ed.), Methods of enzymatic analysis, 2nd ed. New York Academic Press, New York, NY.
63. **Winder, W. W., and D. G. Hardie.** 1999. AMP-activated protein kinase, a metabolic master switch: possible roles in type 2 diabetes. Am. J. Physiol. **277:**E1–E10.
64. **Yoon, J. C., P. Puigserver, G. Chen, J. Donovan, Z. Wu, J. Rhee, G. Adelmant, J. Stafford, C. R. Kahn, D. K. Granner, C. B. Newgard, and B. M. Spiegelman.** 2001. Control of hepatic gluconeogenesis through the transcriptional coactivator PGC-1. Nature **413:**131–138.
65. **Zhou, Y. T., Z. W. Wang, M. Higa, C. B. Newgard, and R. H. Unger.** 1999. Reversing adipocyte differentiation: implications for treatment of obesity. Proc. Natl. Acad. Sci. USA **96:**2391–2395.